

MASTER'S THESIS 2023

Integration of BECCS to a CHP plant

A comparison between CCS technologies using HPC and MDEA/DEA blend by performing Aspen Plus simulations

BRANKO MARKOVIĆ
LINA HÅKANSSON



CHALMERS
UNIVERSITY OF TECHNOLOGY

Department of Chemistry and Chemical Engineering
Division of Chemical Engineering
CHALMERS UNIVERSITY OF TECHNOLOGY
Gothenburg, Sweden 2023

Integration of BECCS to a CHP plant
BRANKO MARKOVIĆ & LINA HÅKANSSON

© LINA HÅKANSSON & BRANKO MARKOVIĆ, 2023.

Supervisor: Daniel Eidenskog, Växjö Energi AB
Supervisor: Benjamin Storm, IVL Svenska Miljöinstitutet AB
Supervisor: Tomas Rydberg, IVL Svenska Miljöinstitutet AB
Examiner: Diana Bernin, Department of Chemistry and Chemical Engineering

Master's Thesis 2023
Department of Chemistry and Chemical Engineering
Division of Chemical Engineering
Chalmers University of Technology
SE-412 96 Gothenburg
Telephone +46 31 772 10 00

Typeset in L^AT_EX
Printed by Chalmers Reproservice
Gothenburg, Sweden 2023

Integration of BECCS to a CHP plant
LINA HÅKANSSON
BRANKO MARKOVIĆ
Department of Chemistry and Chemical Engineering
Chalmers University of Technology

Abstract

One of the main causes of the ongoing global warming is the increasing carbon dioxide (CO₂) concentration in the atmosphere. This has led to carbon capture and storage (CCS) being regarded as one of the various tools to counter the climate change. In this thesis the implementation of bio energy carbon capture and storage (BECCS) at Växjö Energi AB's (VEAB's) combined heat and power (CHP) plant has been evaluated.

Two different post-combustion CCS technologies were compared with the major difference being the solvent used absorb the CO₂ from the CHP flue gas. One of the technologies uses hot potassium carbonate (HPC) as absorbent solution and the other technology uses a blend of the amines MDEA and DEA. The comparison was performed by simulating the different capture technologies in the software Aspen Plus, where the models also were optimized from an energy usage perspective by performing parameter studies. The comparison was then completed by performing a heat integration of the CCS models to the CHP plant to evaluate how they affected the CHP plant performance.

The results from the Aspen Plus simulations and the heat integration led to the conclusion that the HPC technology seemed to have the better performance and higher integration potential to VEAB's CHP plant.

Keywords: BECCS, CCS, HPC, MDEA, DEA, Aspen Plus, Heat recovery, LVC, ICA

Acknowledgements

We would first like to thank VEAB for giving us the opportunity to do this thesis work. We are especially grateful for Daniel Eidenskog's and Julia Ahlrot's continuous involvement and support throughout the project. A special thanks to you Daniel for your valuable input, encouragement and help with the heat integration. Without you this thesis would not have been possible!

We would also like to thank Tomas Rydberg for taking us in and providing supervision at IVL. We are really grateful for Benjamin Storm's expertise and his engagement for our work. Benjamin's wise words and input increased the quality of this work significantly. We are very grateful for his support and efforts, thank you for everything Benjamin!

Finally, we would also like to acknowledge the help from Tharun Roshan Kumar from the Energy Technology Division at Chalmers. Tharun gave us very valuable information regarding the Aspen Plus simulations, which laid ground for the entire report. Thank you Tharun for taking your valuable time to help us!

Lina Håkansson & Branko Marković
Gothenburg, May 2023

List of Abbreviations

Below is the list of acronyms that have been used throughout this thesis listed in alphabetical order:

AF	Air Factor
AMP	2-amino-2-methyl-1-propanol
BECCS	Bio Energy Carbon Capture and Storage
CC	Carbon Capture
CCS	Carbon Capture and Storage
DEA	Diethanolamine
DH	District Heating
ELECNRTL	Electrolyte Non-random Two-liquid
HEX	Heat Exchanger
HPC	Hot Potassium Carbonate
HP1	Heat Pump 1
HP2	Heat Pump 2
ICA	Intercooled Absorption
IC/L	Intercooling to Liquid Ratio
LP	Low Pressure
LVC	Lean Vapour Compression
LV-Flash	Lean Vapour Flash
L/G Ratio	Liquid to Gas Ratio
MDEA	Methyl Diethanolamine
MEA	Monoethanolamine
PZ	Piperazine
SRK	Soave-Redlich-Kwong
SV2	Sandviksverket 2
SV3	Sandviksverket 3
VEAB	Växjö Energi AB

List of Symbols

η_e	Electrical Efficiency
η_{tot}	Total Efficiency
α	Power-to-Heat Ratio
P_{net}	Net Electricity Production
Q_{fuel}	Energy input to Steam Boiler
Q_{DH}	Total District Heating
K_{eq}	Equilibrium Constant
Q_{Spec}	Specific Heat Duty
Q_{Reb}	Reboiler Duty
M_{CO_2}	Mass Flow of CO ₂
$C_{P_{water}}$	Specific Heat Capacity
Q	Heat Duty
ΔT_{min}	Minimum Temperature Difference
Bar	Absolute Pressure, bar(a)
CO ₂	Carbon Dioxide
CO	Carbon Monoxide
H ₂	Hydrogen
H ₂ O	Water
O ₂	Oxygen
NO	Nitrogen Oxide
NO ₂	Nitrogen Dioxide
NO _x	Nitrogen Oxides
NO ₃ ⁻	Nitrate Ion
KHCO ₃	Potassium Bicarbonate
K ⁺	Potassium Ion
CO ₃ ⁻²	Carbonate Ion
HCO ₃ ⁻	Bicarbonate Ion
OH ⁻	Hydroxide
K ₂ CO ₃	Potassium Carbonate
SO ₂	Sulfur Dioxide
N ₂	Nitrogen Gas
HCl	Hydrochloric Acid
NH ₃	Ammonia
HF	Hydrogen Fluoride

Contents

List of Abbreviations	v
List of Symbols	vi
List of Figures	ix
List of Tables	xii
1 Introduction	1
1.1 Background	2
1.2 Problem Statement and Aim	2
1.3 Scope and Overview	3
2 Theory	4
2.1 Combined Heat and Power (CHP)	4
2.1.1 CHP Efficiency	5
2.1.2 Heat Pump	6
2.2 Carbon Capture and Storage (CCS)	7
2.2.1 Amine Cycle	8
2.2.1.1 Process Mechanisms	9
2.2.1.2 Amine Solvents	10
2.2.2 HPC Cycle	12
2.2.2.1 Process Chemistry	13
2.2.3 Process Optimization	14
2.2.3.1 Addition of Promoters to HPC Process	14
2.2.3.2 Lean Vapour Compression (LVC)	16
2.2.3.3 Intercooled Absorption (ICA)	16
2.2.4 Liquefaction and Purification of CO ₂	17
2.2.5 Geological Storage of CO ₂	19
3 Methodology	20
3.1 Aspen Plus Model Setup	20
3.1.1 Property Methods for Aspen Plus Simulations	20
3.1.2 Flue Gas Data	21
3.1.3 Reactions	22
3.1.3.1 HPC Reactions	23
3.1.3.2 MDEA/DEA Reactions	24
3.1.4 Column Model Setup	25

3.2	Process Modelling	26
3.2.1	HPC Model	27
3.2.2	MDEA/DEA Model	29
3.2.3	Liquefaction Model	30
3.3	Heat Integration	30
3.3.1	HPC	31
3.3.2	MDEA/DEA	31
3.3.3	Liquefaction	31
4	Parameter Study & Model Optimization	32
4.1	HPC Parameter Study	32
4.1.1	Absorber Pressure	32
4.1.2	Desorber Pressure	33
4.1.3	Absorber Inlet Temperature	34
4.1.4	Lean Solvent Loading	35
4.1.5	Lean Solvent K_2CO_3 Concentration	36
4.1.6	L/G Ratio (Semi-Locked)	36
4.1.7	Lean Vapour Compression (Atmospheric LV-Flash)	37
4.1.8	Lean Vapour Compression (Sub-atmospheric LV-Flash)	37
4.1.9	Optimized HPC Model	38
4.2	MDEA/DEA Parameter Study	40
4.2.1	Desorber Pressure	40
4.2.2	Lean Solvent Temperature	41
4.2.3	Lean Solvent Loading	42
4.2.4	Lean Solvent MDEA/DEA Composition	42
4.2.5	L/G Ratio (Semi-Locked)	44
4.2.6	Lean Vapour Compression	44
4.2.7	Intercooling	45
4.2.8	Optimized MDEA/DEA Model	47
5	Heat Integration	49
5.1	Heat Integration within CCS	49
5.2	Integration of CCS to the CHP Plant	50
5.2.1	Full Load	50
5.2.2	Half Load	52
5.3	Heat Integration Summary	54
6	Conclusions	55
6.1	Future Work	55
A	Liquefaction Model in Aspen Plus	I
B	Heat pump data & pictures from heat integration	III
C	CHP data for SV2 and SV3	V
D	Specific Heat Duties from Literature	VII

List of Figures

2.1	Process diagram of a general CHP steam turbine cycle.	5
2.2	Simplified process diagram of a general CCC heat pump.	6
2.3	General post combustion chemical absorption cycle using the temperature swing principle.	8
2.4	General post combustion chemical absorption cycle using the pressure swing principle.	13
2.5	General scheme of lean vapour compression.	16
2.6	General scheme of intercooled absorption.	17
2.7	Pressure-temperature phase diagram for CO ₂	18
3.1	Aspen Plus HPC base case model.	28
3.2	Aspen Plus MDEA/DEA base case model.	29
4.1	Reboiler duty as a function of absorber pressure.	32
4.2	Compander net duty as a function of absorber pressure.	32
4.3	L/G ratio as a function of absorber pressure.	33
4.4	Net duty cost as a function of absorber pressure.	33
4.5	Specific heat duty as a function of desorber pressure.	33
4.6	Reboiler duty as a function of absorber temperature.	34
4.7	Compander net duty as a function of absorber temperature.	34
4.8	L/G ratio as a function of absorber temperature.	34
4.9	Net duty cost as a function of absorber temperature.	34
4.10	Specific heat duty as a function of lean solvent loading.	35
4.11	L/G ratio as a function of lean solvent loading.	35
4.12	Specific heat duty as a function of lean solvent K ₂ CO ₃ concentration.	36
4.13	Absorber efficiency as a function of the L/G ratio.	36
4.14	Reboiler duty as a function of lean vapour compressor discharge pressure.	37
4.15	Lean vapour compressor duty as a function of discharge pressure.	37
4.16	Duty cost as a function of LVC & desorber pressure.	38
4.17	Aspen Plus optimized HPC model.	40
4.18	Specific pump duty as yellow line (left axis) and specific heat duty as orange line (right axis) as a function of desorber pressure.	40
4.19	Specific heat duty as a function of lean in temperature to the absorber, with the black line represents the base case.	41
4.20	L/G Ratio as a function of lean in temperature to the absorber, with a black line represents the base case.	41
4.21	Rich loading as a function of lean in temperature to the absorber, with a black line represents the base case.	41

4.22	Specific heat duty as a function of lean solvent loading, with a black line represents the base case.	42
4.23	L/G Ratio as a function of lean solvent loading, with a black line represents the base case.	42
4.24	Specific heat duty as a function of lean loading for different MDEA/DEA mixtures.	43
4.25	Specific heat duty as a function of lean loading for different MDEA/DEA mixtures, zoomed in.	43
4.26	Absorber efficiency as a function of L/G Ratio, with a black line represents the base case.	44
4.27	Specific heat duty as a function of LV-flash pressure.	44
4.28	Specific compander duty as a function of LV-flash pressure.	44
4.29	Total duty cost as a function of LV-flash pressure.	45
4.30	Specific heat duty as a function of intercooling ratio (IC/L).	45
4.31	Rich Loading as a function of intercooling ratio (IC/L).	45
4.32	Specific heat duty for different intercooling stages using 60% IC/L	46
4.33	Aspen Plus MDEA/DEA optimized model.	47
A.1	Liquefaction model used for the HPC and MDEA/DEA models to obtain power and cooling need.	II
B.1	Aspen Plus Heat Pump 1 model.	III
B.2	Aspen Plus Heat Pump 2 model.	IV
C.1	Data for SV3 - District heating output (MW) vs load	V
C.2	Data for SV3 - Power output (MW) vs load	V
C.3	Data for SV2 - District heating output (MW) vs load	VI
C.4	Data for SV2 - Power output (MW) vs load	VI

List of Tables

3.1	Unconverted flue gas data from VEAB.	21
3.2	Flue gas data input into Aspen Plus for full load and half load.	22
3.3	Reactions registered in Aspen Plus for absorption and desorption in the HPC cycle [34].	23
3.4	Equilibrium coefficients for Reactions 1-3 in Table 3.3 [34].	23
3.5	Kinetic constants for Reactions 4-5 in Table 3.3 [34].	23
3.6	Reactions registered in Aspen Plus for absorption and desorption in the MDEA/DEA cycle [35].	24
3.7	Equilibrium coefficients for Reactions 1-6 in Table 3.6 [35].	24
3.8	Kinetic constants for Reactions 7-12 in Table 3.6 [35].	24
3.9	Column settings for base case model setup.	25
3.10	HPC base case model settings.	28
3.11	HPC base case model results.	28
3.12	MDEA/DEA base case model settings.	29
3.13	MDEA/DEA base case model results.	29
4.1	HPC optimized downsized model settings.	38
4.2	HPC optimized downsized model results.	39
4.3	MDEA/DEA optimized downsized model settings.	47
4.4	MDEA/DEA optimized downsized model results.	48
5.1	Heat integration for MDEA/DEA capture process.	49
5.2	Heat integration for HPC capture process.	49
5.3	Result from heat integration for full load (winter case), assuming DH demand of 119.7 MW.	51
5.4	Result from heat integration for half load (summer case), assuming DH demand of 17.5 MW.	53
B.1	Result from MDEA/DEA heat integration of Heat Pumps.	IV
D.1	Specific heat duty for solvent regeneration for MEA, MDEA, DEA and HPC capture technologies based on literature.*Uses pressurized absorption VII	

1

Introduction

The carbon dioxide (CO_2) concentration in the atmosphere is drastically increasing due to human activities. The annual increasing rate of CO_2 over the past 60 years has been around 100 times faster than previous natural increases. Action must be taken in order to minimize the global effects of the atmospheric CO_2 increase [1].

CO_2 is a gas that absorbs and radiates heat, i.e. a greenhouse gas. When the sun shines on earth, heat is radiating back from the earth's surface. This heat is absorbed by the greenhouse gases in the atmosphere and then released in all directions, including back to the earth surface. This is the natural greenhouse effect and it is vital in order to keep the surface temperature above freezing [1]. However, due to the increasing use of fossil substances, more carbon has been fed into the carbon cycle giving rise to more CO_2 in the atmosphere. Hence, the current greenhouse effect is not natural and causing the global temperature to rise resulting in unwanted environmental effects all around the world.

Out of all human activities, utilization of fossil fuels for energy are one of the main causes for the rising CO_2 concentration in the atmosphere [1]. This makes it vital to investigate and develop technologies that aim to decrease or stop the emissions of CO_2 from industries. One way to tackle this is to implement Carbon Capture and Storage (CCS). CCS consists of three main parts, first the CO_2 must be captured at site, then the captured CO_2 is liquified and lastly stored in geological reservoirs. By permanently storing the captured CO_2 , the carbon is removed from the carbon cycle and the atmosphere. If biogenic fuel would be used instead, it is possible to obtain net negative emissions. Bio-energy carbon capture and storage (BECCS) is therefore a very important tool in the effort to prevent and stop the global warming.

Carbon capture technologies can be divided into three main categories: pre-combustion, oxy-fuel combustion and post-combustion. The categorizing depends on how and when the CO_2 is captured in the process. This thesis will focus on technologies that capture CO_2 after combustion, i.e. post-combustion, due to their easy implementation in both new and existing plants. However, post-combustion capture technologies do have one downside, they often demand a large amount of energy which results in decreased efficiency of the power plant [2]. Therefore, it is vital to investigate how this energy demand can be decreased and how the implemented technology affects the plant performance. If the energy penalty could be decreased, also the incentive to implement CCS would be increased, which would limit or even decrease the CO_2 concentration in atmosphere.

1.1 Background

This master thesis is in collaboration with Vaxjo Energi AB (VEAB) which are responsible for supplying district heating and electricity for residents in Vaxjo municipality. VEAB uses forest residues to fuel their combined heat and power (CHP) plant, thus giving rise to biogenic CO₂ emissions. VEAB has a long-term goal to integrate a carbon capture technology into their CHP plant by 2027, which could result in net negative emissions due to their use of biogenic fuel. Their CHP plant consists of two blocks: Sandvik 3 (SV3) and Sandvik 2 (SV2). The idea is to implement CCS to SV3, their main production block, while SV2 acts as a peak load boiler during winter and as main boiler during maintenance stops at SV3. Thus, this thesis will focus on the implementation of the following capture technologies onto SV3: Hot potassium carbonate (HPC) cycle and an amine-solvent capture technology.

1.2 Problem Statement and Aim

The main obstacle with implementation of CCS is the energy demand of the CO₂ capture. Thus, in order to make CCS feasible to implement, the capture technology must be energy and cost efficient. It is therefore vital to investigate how different parameters affect the capture technologies' energy demand and how the energy can be heat integrated into the district heating network.

The goal with the thesis is to contribute to the search after the most optimal carbon capture technology. The aim is to compare two capture technologies by evaluating their effect on VEAB's CHP plant performance. Both of the capture technologies are chemical absorption based where one technology uses HPC and the other uses an amine blend as absorption solvent. The ambition is to make credible Aspen Plus models of the capture technologies and to evaluate their performance regarding energy demand, heat integration possibilities and efficiency. Additionally, the CCS performance during winter season and summer season will be investigated to evaluate their resistance to changing seasons. More specifically, the following questions will be answered:

- Which carbon capture technology has the best performance and integration potential to VEAB's CHP plant?
- Which process conditions for the carbon capture technologies are favourable in order to minimize the need of external energy duties?
- How are the capture technologies' performance and heat integration possibilities affected by full CHP load (winter season) vs half CHP load (summer season)?

1.3 Scope and Overview

The thesis includes a literature study where different carbon capture technologies are investigated regarding their advantages and limitations. The two most relevant capture technologies, HPC and amine-solvent capture, are investigated in more detail regarding their chemistry and process mechanisms. Also, a suitable amine solvent is proposed.

Process simulations were performed in Aspen Plus to evaluate the performance of the carbon capture technologies, if implemented on VEAB's CHP plant. Different operating conditions and parameters were tested in order to meet VEAB's requirement of 90% CO₂ capture rate while minimizing the energy demand. Moreover, a liquefaction process was simulated to meet VEAB's specified output of liquefied CO₂ at 16 bar and -28°C. Note that all pressures presented in the thesis are indicated as absolute pressures. As an addition to process simulations, heat integration possibilities are investigated for each technology. The heat integration study investigates how the excess energy from the capture processes could be utilized in district heating. Thus, the heat integration study helps evaluating the influence CCS would have on VEAB's CHP plant performance.

The thesis does not include any simulations of VEAB's CHP plant. Instead flue gas data from VEAB constituted the basis of the Aspen Plus simulations, which only included simulations of the carbon capture technologies and liquefaction. Also, no in depth investigations regarding economic feasibility or the storage/transport of the liquefied CO₂ was performed in this thesis. Only a simple duty cost evaluation was made when comparing the different technologies and CHP loads.

2

Theory

The theory covers the literature study and the basic topics concerning this thesis. The chapter starts with a comprehensive description of what a combined heat and power plant is and what it is used for. Then, the theory moves on to the principle behind carbon capture and storage. In this section, a detailed description of the two CO₂ capture technologies treated in this thesis is provided. The topics covered are the general tendencies, advantages, limitations and process mechanisms of the technologies. For the amine technology, different solvents are evaluated based on literature and a suitable amine solvent is suggested. The final part of the theory covers the basics of liquefaction and storage of CO₂.

2.1 Combined Heat and Power (CHP)

Combined heat and power (CHP) is a technology which produces both electricity and thermal energy simultaneously. The main benefit with a CHP is that a very large portion of the energy stored in the fuel is being utilized [3]. There are various types of designs for a CHP plant, but a general layout is the steam turbine cycle, i.e. the Rankine cycle. In the steam turbine, cycle water is evaporated into superheated steam in a furnace, which could be fired by various types of fuels. The superheated steam is then expanded in a turbine, which drives a generator that produces electricity. After the steam has been expanded, the remaining energy is utilized to heat the water used for district heating (DH). The steam gets condensed and then pumped back into the furnace and then the cycle is repeated. The furnace that drives the CHP can be operated at different loads to meet the desired power or/and DH output that changes over the year. The load can be changed by adjusting the fuel input, hence its maximum capacity corresponds to full load and half its capacity corresponds to half load [3]. A simplified process diagram of the steam turbine cycle can be seen in Figure 2.1.

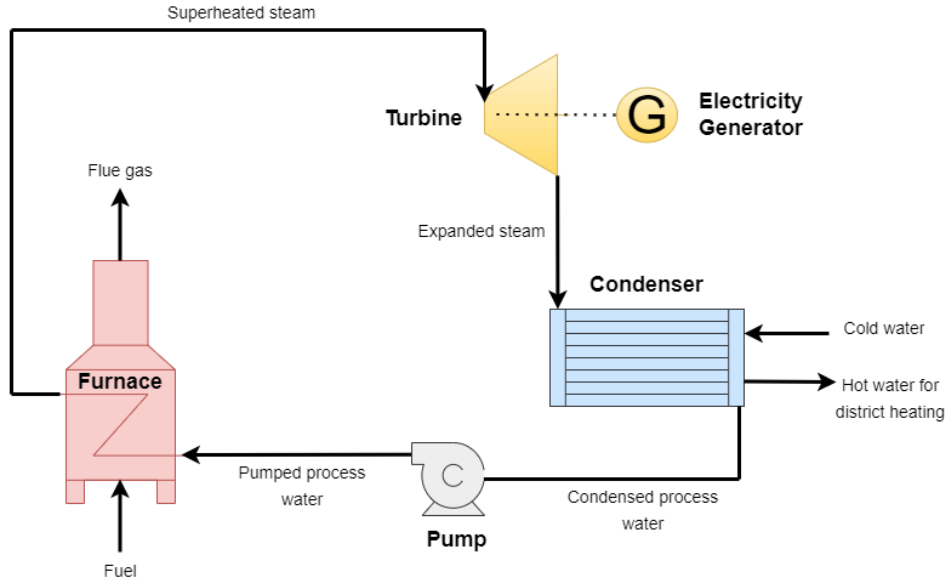


Figure 2.1: Process diagram of a general CHP steam turbine cycle.

Depending on the plant and possible industrial symbiosis involvements, there could be multiple extraction points of the steam at different pressure levels. Processes like CCS are in general very energy demanding, which could lead to the requirement of using a portion of the produced steam to cover energy duties within the process [2].

2.1.1 CHP Efficiency

When implementing an energy demanding CCS technology that is integrated to the CHP plant it is important to observe the changes in the efficiency factors when determining the feasibility of a certain technology. If the technology demands relatively large amounts of energy it could lead to large reductions in the efficiency factors, since less of the energy available in the fuel is used produce heat and electricity. Usually, between 65% to 90% of the energy in the fuel is utilized in a CHP plant without any CCS technology integrated [4]. However, with a flue gas condenser an efficiency of 110% can be obtained [5].

In order to determine the efficiency of a CHP plant there are certain parameters that can be observed. The electrical efficiency, η_e , is defined as:

$$\eta_e = \frac{P_{net}}{Q_{fuel}} \quad (2.1)$$

where P_{net} is the net electricity production and Q_{fuel} is the total amount of energy input to the boiler from the fuel.

However, since the energy in the expanded steam is utilized for DH the total efficiency, η_{tot} , is of larger relevance. It is defined as:

$$\eta_{tot} = \frac{P_{net} + Q_{DH}}{Q_{fuel}} \quad (2.2)$$

where Q_{DH} is the total district heat produced.

Another interesting parameter to observe is the power-to-heat ratio, α , which is defined as:

$$\alpha = \frac{P_{net}}{Q_{DH}} \quad (2.3)$$

The power-to-heat ratio describes the ratio between the produced electricity and the produced district heating from the available energy in the steam [6].

2.1.2 Heat Pump

In a carbon capture process there are various streams that have different temperatures, which may need either cooling or heating. The optimal solution would be to integrate heat within the process, or use excess heat for other purposes. In the case when a carbon capture process is integrated to a CHP plant it would be a favourable solution to use excess heat for district heating. However, in some cases certain streams that require cooling might not have sufficiently high temperatures to use their excess heat for district heating. Then it would be fitting to introduce a heat pump.

The working principle of a heat pump is that it transfers heat from a low temperature heat source to a high temperature heat sink. For this to be possible an external energy input is required, often in the form of work [7]. In Figure 2.2 a process diagram of a simple closed compression cycle heat pump can be observed. Within the closed cycle usually a refrigerant such as R134a or ammonia, etc. is used to transfer the heat from the source to the sink [7].

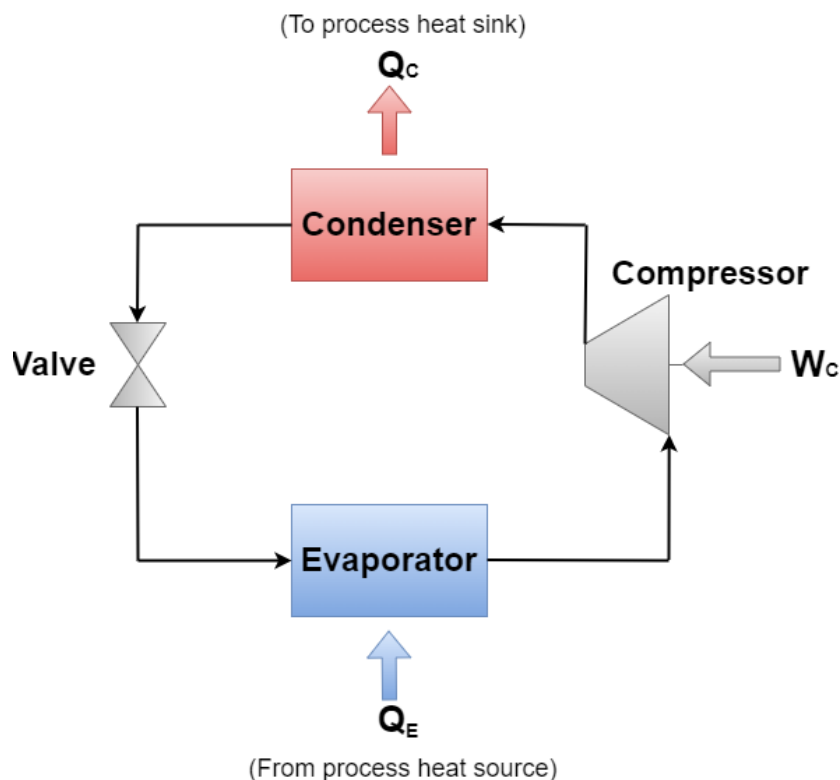


Figure 2.2: Simplified process diagram of a general CCC heat pump.

2.2 Carbon Capture and Storage (CCS)

The idea with the CCS is to capture the CO_2 at site, after which it is liquefied and purified, and lastly stored in closed reservoirs. In this way, the CO_2 is removed from the carbon cycle and will not contribute to the environmental effects associated with global warming. This enables possibilities to obtain neutral or negative emissions depending on the fuel used.

There are three main technologies to capture CO_2 : pre-combustion, oxy-fuel combustion and post-combustion. In pre-combustion, the CO_2 is removed before the combustion is complete. First, the fuel goes through the gasifier which converts the fuel to CO and H_2 . Then, by using the water-gas shift reaction, the CO is converted to CO_2 . This stream will have high partial pressure of CO_2 , making it relatively easy to remove. The H_2 that is left, after CO_2 capture, will go through combustion to generate power [8]. The advantage with pre-combustion is the high partial pressure of CO_2 and the main disadvantage is its equipment complexity, which could be difficult to implement on an existing plant [2].

Oxy-fuel combustion uses pure oxygen to combust the fuel, which results in CO_2 and H_2O being the primary combustion products [8]. The advantages with oxy-fuel combustion are that no chemicals are used and that it has better heat transfer properties than the other mentioned technologies. However, it is a quite new technology and has thus mainly been demonstrated on small scale and special cases. In addition, pure O_2 is costly and large quantities is needed, which also speaks against using oxy-fuel combustion [2].

In post-combustion capture technologies, the CO_2 is captured after combustion by separating the CO_2 from the flue gases [8]. The main advantage with this technology is its flexibility since it can quite easily be fitted into both new and old plants. The main disadvantage is the high energy penalty that this technology generally gives rise to [2]. Since an existing CHP plant is in focus, a post-combustion technology is considered to be the most relevant since that would minimize changes to the existing plant and its' units. Hence, only post-combustion capture technologies will be further evaluated.

Various post-combustion capture technologies exist, but the most discussed and known technologies are chemical solvent absorption, solid sorbent adsorption, cryogenic distillation and membrane separation. The most commercialized and mature technology of these is the chemical solvent absorption technology. The matureness, together with its high selectivity and high absorption efficiency is the reason to why chemical absorption technologies will be the main focus in this thesis [9].

The chemical absorption technology uses a solvent to selectively absorb CO_2 in a gas-liquid contact system, i.e. an absorber. Then, the solvent is regenerated in the desorber by supplying energy in the reboiler. In general, there are two main categories of solvents. The first category is organic solvents, which include alkanolamines like monoethanolamine (MEA), diethanolamine (DEA) and methyl diethanolamine (MDEA). The second category is inorganic solvents, which include solvents like potassium carbonate (K_2CO_3). Generally, inorganic solvents have a lower price, fewer environmental effects and higher stability than organic solvents. However, inorganic solvents have poorer selectivity towards CO_2 than organic ones [10]. This thesis will investigate the inorganic hot potassium carbonate (HPC) cycle technology and the organic amine-solvent capture technology.

2.2.1 Amine Cycle

Carbon capture using amine solvents is considered to be one of the most promising post-combustion capture technologies due to its maturity, cost effectiveness and capacity to handle large flue gas streams [9]. The amine-solvent capture technology is based on the temperature swing principle. In the temperature swing principle the CO_2 is absorbed in low temperatures and then desorbed at higher temperatures [11]. Thus, the technology consists of one absorber and one desorber supported by equipment like reboiler, condenser and heat exchanger. Figure 2.3 represents a general amine-based temperature swing technology.

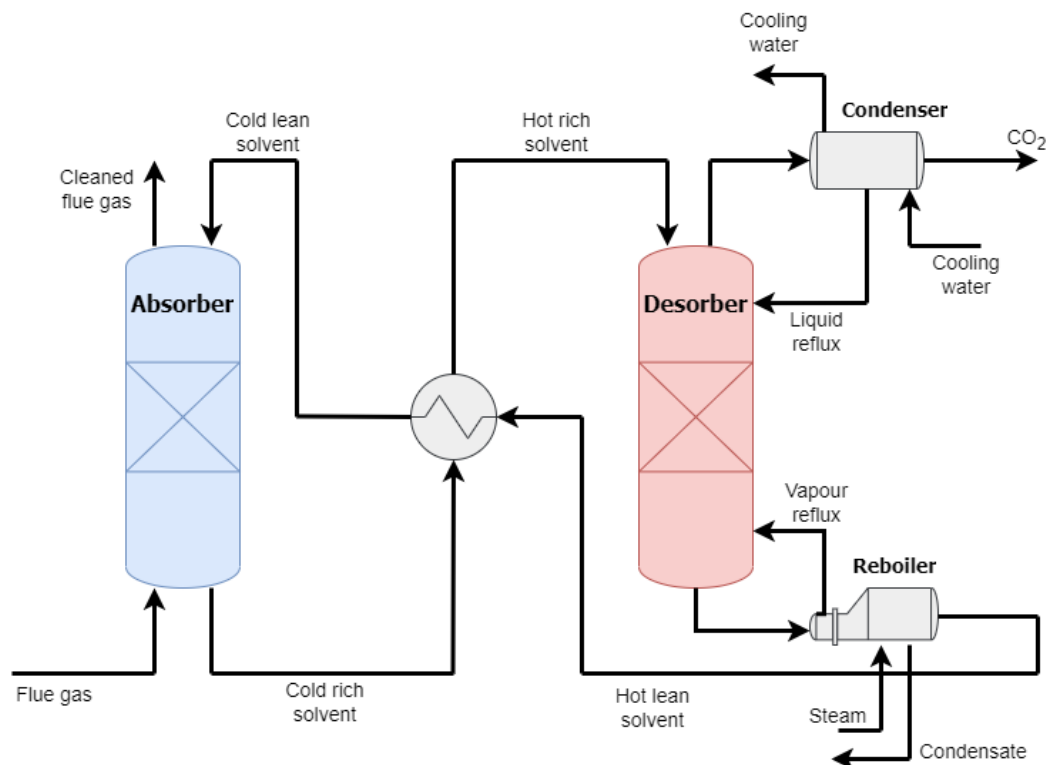


Figure 2.3: General post combustion chemical absorption cycle using the temperature swing principle.

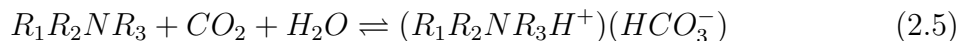
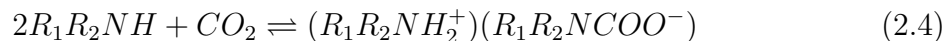
The cycle in Figure 2.3 begins with the flue gas from the combustion entering the absorber which contains an amine solution that absorbs the CO_2 . The CO_2 -rich solution, leaving the absorber, is pre-heated in a cross-section heat exchanger before entering the desorber [12]. In the desorber, the solution is heated with the reboiler to release the absorbed CO_2 . The lean amine leaving the desorber is used in the heat exchanger to pre-heat the rich amine stream before being re-used in the absorber. When re-using the amine solution, the solvent goes through periodic heating and cooling. As time goes by, the amine solutions start to degrade due to thermal and oxidative reaction mechanisms [11]. Thus, the solvent must be periodically replaced with make-up amine in order to maintain the capture performance.

Even though this technology is said to be well-developed and considered to be the cheapest post-combustion CO_2 capture technology, there are still some issues. The high temperature of the flue gas can cause thermal degradation and evaporation of the amine solutions due to their high volatility, risking severe amine losses [12]. In addition, amines could cause problem to process equipment due to their corrosiveness. There is also an energy penalty in the desorber for regenerating the amine solution, leading to decreased efficiency of the CHP plant.

Another general but serious issue with amines needs to be pointed out. When the nitrogen oxide (NO_x) containing flue gas enters the absorber, nitrogen dioxide (NO_2) can be dissolved in the amine solvent. NO_2 then produces a nitrate ion (NO_3^-) which reacts with the amine to form nitrosamines [13]. Nitrosamines are classified as possible carcinogens, based on animal studies, which makes it a potential hazard [14]. There is not only a risk of NO_3^- formation in the absorber, but also in the desorber. NO_3^- can be created in the desorber due to oxidative degradation of the solvent, which then further reacts with secondary amines to form nitrosamines when CO_2 is present. Even though secondary amines might not be present at first, they can be created due to thermal and oxidative degradation pathways [13]. Hence, degradation products of amines could be a potential threat to the environment and inhabitants near the plant. Due to time limitations, these nitrosamine formation reactions will not be modelled in the Aspen Plus simulations.

2.2.1.1 Process Mechanisms

The absorption mechanism occurring at the gas-liquid interface can be explained with the film theory. At the interface, the gaseous CO_2 is dissolved in the solvent while some of the solvent evaporates to the gas phase, resulting in molecules from both phases migrating between the bulk and interface [15]. When CO_2 (g) near the g/l-interface is dissolved into the solution, a concentration gradient is formed. The concentration gradient gives rise to a migration of bulk CO_2 (g) to the interface. When the dissolved CO_2 meets amine molecules in the liquid, a chemical reaction occurs. Since the CO_2 concentration in the liquid is decreased, more CO_2 can be dissolved into the liquid [15]. This migration is therefore driven by diffusion transport, which is influenced by the reaction rate and liquid properties like viscosity and temperature [15]. The reactions between CO_2 and amines are exothermic and occur mainly through two reactions: carbonate formation (2.4) and bicarbonate formation (2.5) [15]:



In primary amines, R_1 is hydrogen while R_2 is an organic substituent. In secondary amines, neither R_1 or R_2 are hydrogen but instead organic substituents. Hence, both Reaction 2.4 and 2.5 are possible for primary and secondary amines. However, for a tertiary amine none of the substituents (R_1, R_2, R_3) are hydrogen, thus only bicarbonate formation (Reaction 2.5) is possible. To enable regeneration of the amines, the solution is heated to drive the equilibrium towards the reactants in (2.4) and (2.5), using the temperature swing principle [12]. Since water is an essential component of amine solutions, which has a basic pH, also the following reactions occur within the system [15]:



2.2.1.2 Amine Solvents

Two important absorbent properties to evaluate are the oxidative degradation and the amine volatility. The oxidative degradation is mainly an issue if the flue gas contains oxygen. A high oxygen degradation results in a high decomposition rate of amine and thereby amine losses. If the amine has a high volatility, there are also losses to the environment [15]. As stated in Section 2.2.1, the release of these amines and their degraded components could have possible health and environmental effects. However, alkanolamines which are commonly used for CO_2 capture, have a generally low environmental impact. If emitted to the atmosphere, alkanolamines have shown to be removed by reactions with photochemically generated hydroxyl radicals [16]. Also, alkanolamines are susceptible to biodegradation in soil, surface waters and wastewater, and thus not expected to persist in the environment [16]. In addition, alkanolamines have a relatively low price, acceptable rate of reaction, relatively high availability and high stability [17]. Therefore, alkanolamines will be the in the focus when choosing a suitable amine-solvent for CO_2 capture at VEAB's site.

Alkanolamines is an amine family that consists of ethanol-, isopropanol- and butanol substituted amines. They can be divided into three different groups: primary (RNH_2), secondary (R_2NH) and tertiary amines (R_3N). Regarding CO_2 capture, primary amines like monoethanolmine (MEA) and secondary amines like diethanolamine (DEA) have high reaction rates [9]. However, these amines have drawbacks like low CO_2 capacity (0.5 mol CO_2 /mol amine) and high energy consumption for regeneration. Tertiary amines like methyl-diethanolamine (MDEA) have generally lower reactivity with CO_2 but a lower energy penalty for regeneration and higher loading capacity (1 mol CO_2 /mol amine) [9]. There are also specialty amines, like the steric hindered 2-amino-2-methyl-1-propanol (AMP) and the cyclic diamine piperazine (PZ) that has shown promising result regarding CO_2 capture.

Hence, there is a trade-off when choosing between these alkanolamines. Amine solvents with efficient absorption give rise to a high energy penalty for regeneration due to their stronger absorption. While an amine with low reactivity has a low energy penalty due to more efficient desorption as a result of weaker absorption. There is no extraordinary amine that can provide a solution for all the problems associated with the technology. But, the most interesting options for this thesis are MEA, DEA and MDEA since they are the most frequently used amines commercially. Hence, they would be realistic amine solvents to implement at VEAB's site. Despite that MDEA has lower reactivity than MEA and DEA, MDEA has more advantages due to its higher CO_2 loading capacity, lower pressure requirement, higher boiling point and lower energy penalty [18]. In addition, MDEA does not possess as harsh corrosive properties, thus preserving the equipment from damage [10]. The previously mentioned points make MDEA the most interesting single-solvent for this thesis.

A more promising option is to use a mixture of amines as a solvent for the CO_2 capture. A mixture makes it possible to combine advantages of multiple amines to enhance the capture performance while increasing the loading capacity, making the solvent more chemically stable and increasing the reactivity [10]. Since MDEA mostly lacks regarding the reactivity with CO_2 , an option would be to include an amine with higher reactivity. According to literature PZ, MEA or DEA would be good reactivity promoters due to their higher reaction rates and faster reaction kinetics with CO_2 [9]. PZ is the amine with the most promising general properties and reaction kinetics, but it exhibits a higher risk for harming employees. Unlike MEA and DEA, PZ can cause severe allergy, asthma and could be a potential threat for fertility and fetuses [19]. To avoid this potential hazard, PZ is discarded as a potential promoter in this thesis. Nevertheless, both MEA and DEA have shown promising reaction promoting properties whileas DEA has shown to have better performance regarding lower regeneration energy [20]. In addition, the research regarding CO_2 capture using MEA and MDEA mixtures are already quite extensive in literature. Hence, the potential of using an MDEA and DEA blend will be investigated in this thesis.

2.2.2 HPC Cycle

The principle of the hot potassium carbonate (HPC) cycle is similar to the amine-based cycles since it is a post-combustion chemical absorption technology. There are various benefits with using HPC as a solvent. Compared to other post-combustion absorption technologies it is relatively cheap and easy to regenerate the solvent due to its low heat of regeneration. The toxicity of HPC is lower than for amines, which corresponds to a lower hazard. In the case of leakage into the environment, the risk is thus smaller due to the decreased hazard compared to other amine-based solvents [21]. Additionally, HPC is less volatile than amines which in the case of leakage reduces the risk due to the lower exposure levels [22]. Other benefits with using HPC as a solvent is that it is less susceptible to oxidative degradation making it rather durable, as well as the lack of possessing corrosive properties [21]. However, there are also disadvantages with implementing the HPC cycle instead of a process using an amine as a solvent. Compared to amine-based solvents, the efficiency of absorbing CO_2 for HPC is rather low, resulting in poor kinetic properties. This results in that HPC often requires larger equipment, which corresponds to higher capital costs. The efficiency can however be improved by various means, such as adding promoters to the solution to enhance the reaction kinetics. Another option is also to streamline the mass transfer in the column by optimizing the packing [23].

The conventional process of capturing CO_2 using HPC as a solvent was developed in the middle of the 20th century and it is called the Benfield process, after the creators Benson and Field. As previously mentioned, the HPC cycle is more energy efficient compared to amine-based alternatives. This is due to the absorption being performed at elevated temperature and pressure levels, which diminishes the need of any heating duty before the regeneration of the solvent in the desorber. The high pressure does also allow for higher solubility of CO_2 [24]. An absorption cycle where the absorption and desorption occur at different pressures is called a pressure swing cycle, which is illustrated in Figure 2.4.

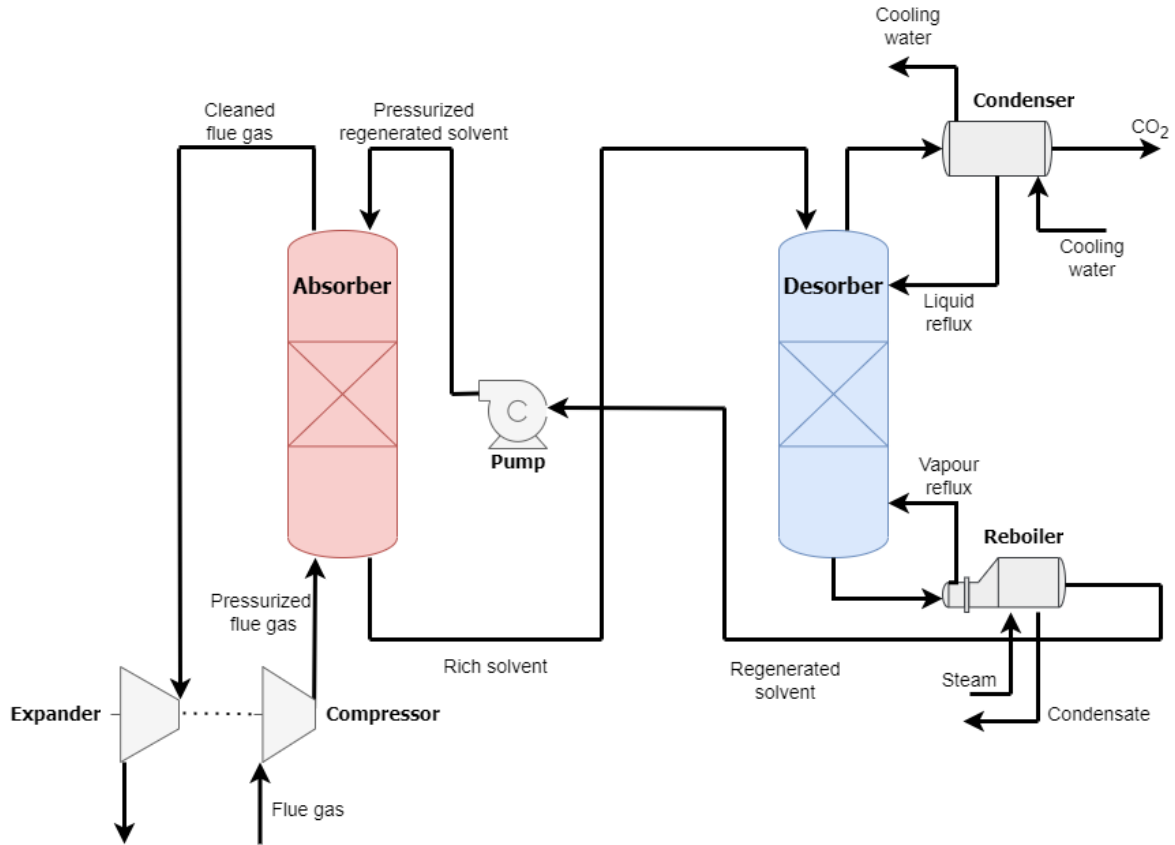


Figure 2.4: General post combustion chemical absorption cycle using the pressure swing principle.

In order to achieve the CO₂ capture with a reasonable equipment size, a high pressure absorber is required. To obtain a sufficient pressure a relatively large compressor is needed to pressurize the incoming flue gas, which demands a lot of electricity. However, since the gas that exits the absorber is pressurized and is relatively warm it contains a considerable amount of energy, which can be utilized by expanding the gas stream. By connecting a shaft between the expander and the compressor a certain amount of work can be recovered, which diminishes the electricity demand in the compressor. This setup where a downstream expander is connected to an upstream compressor is called a compander, which can be seen in Figure 2.4 above.

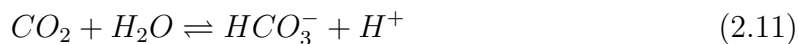
2.2.2.1 Process Chemistry

In an HPC cycle, including both the absorption and desorption, the overall reaction can be expressed as:



In the absorber, the HPC (K₂CO₃) reacts with CO₂ and H₂O forming potassium bicarbonate (KHCO₃), i.e. Reaction (2.10) above goes from left to right. In the desorber, where the HPC is regenerated and CO₂ is separated, the reaction goes from right to left [24].

However, the chemistry can be expressed with a higher degree of detail. Both the potassium carbonate and bicarbonate are electrolytes, hence it can be assumed that the potassium only exists as a K^+ cation in the solution. This would mean that the carbonate and bicarbonate would be expressed as their respective anions in the forms of CO_3^{2-} and HCO_3^- in Reaction (2.10). Based on this, Reaction (2.10) can be expressed as the following reactions which occur simultaneously [24]:



Reactions (2.11) and (2.12) are then instantaneously succeeded by the following reactions:



The pH is usually held at a basic level in industrial absorption operations, which makes Reactions (2.11), (2.13) and (2.14) negligible when it comes to deciding the rate determining reaction. Since Reactions (2.13) and (2.15) are instantaneous, it results in Reaction (2.12) being the rate determining step of CO_2 absorption in the HPC cycle [24].

2.2.3 Process Optimization

A CCS process can be optimized in various ways in order to minimize the external energy duties. Depending on which type of CCS process that is used, different optimization operations can be performed. In the following sections various types of process optimizations for both the HPC process and the amine process are presented.

2.2.3.1 Addition of Promoters to HPC Process

In Section 2.2.2 it was described that a CO_2 absorption process using HPC has inferior kinetic properties compared to technologies using amines. One of the proposed solutions to the problem would be to add so called promoters to the absorbent solution. There are various types of compounds that can be added to the solution in order to promote the CO_2 absorption kinetics. Arsenite, boric acid and vanadate are examples of inorganic compounds that have promoting properties. Also amines such as PZ, MEA and DEA are examples of organic compounds that possess promoting properties. There are also some enzymes that possess promoting properties [23].

Arsenite is a very good promoter of CO_2 absorption in an HPC cycle as it neutralizes the acidity of CO_2 as well as constituting the formation of a CO_2 base complex. However, it is not used in industry due to its carcinogenic and toxic properties. Boric acid is another option that per contra does not constitute an environmental threat. In addition, boric acid is relatively cheap and persistent to degradation in the operating conditions. The downside with boric acid as a promoter is the non-sufficient promoting performance. Vanadate is another inorganic compound that has been evaluated for its promoting properties, but it has been concluded that it is not effective enough.

However, it could still be feasible to add it into the solvent for its corrosion preventing features [23].

The addition of MEA as a promoter to the HPC solution would streamline the CO₂ absorption. The concentration of OH⁻ would increase, which would lead to more CO₂ reacting with OH⁻. The CO₂ absorption would also be enhanced as a result of the zwitterion mechanism which would be induced from the reaction between the MEA and CO₂. Another promoter which performs at similar levels as MEA is PZ, which in addition has a low vapour pressure, low corrosivity and low potential of degradation. However, as mentioned in Section 2.2.1.2, PZ is hazardous to human health and should thereby be treated accordingly. Amines have in general more or less good promoting features for an HPC absorption cycle. However, the addition of any amine would increase the energy duty for the solvent regeneration, which makes it important to carefully examine the potential trade-off between improved kinetics and energy penalty before implementation. Also, since amines are relatively volatile it would result in an additional risk to use them in a pressurized absorption column [23].

In summary, all the promoters mentioned do to a certain extent catalyse the hydration of CO₂, i.e. the reaction between H₂O and CO₂, which speeds up the CO₂ absorption rate in the grand scheme of things. By reacting with H₂O the promoter gets deprotonated and thereby activated. The activated promoter then reacts with CO₂ which forms an intermediate, which eventually reacts with H₂O forming a regenerated promoter and a bicarbonate cation. The entire mechanism is presented in Reactions 2.16, 2.17 and 2.18 below [23].



However, in the performed process simulations there will be no promoter used in the HPC process in order to simplify the simulations. Also, the purpose of the thesis is to compare HPC to an amine solvent, so by using an amine as a promoter would not provide as valuable results.

2.2.3.2 Lean Vapour Compression (LVC)

The warmest part of the desorber column is the last stage where the reboiler is located. The regenerated solvent leaves the column via the reboiler and thereby the stream contains a relatively large amount of energy. By operating the desorber at a pressure slightly above atmospheric pressure and then valve throttling the regenerated solvent it will lead to a portion of the water in the stream evaporating. A larger pressure change will lead to more water evaporating, hence a higher desorber pressure leads to more water evaporating into steam after throttling. The steam can then be re-compressed to the desorber pressure and then be recycled into the reboiler. This leads to a lower demand of excess steam to operate the reboiler and thereby a lower energy penalty for the solvent regeneration. This process modification is called lean vapour compression (LVC) [25] and its implementation will be investigated for both capture technologies. A general scheme of LVC is visualized in Figure 2.5.

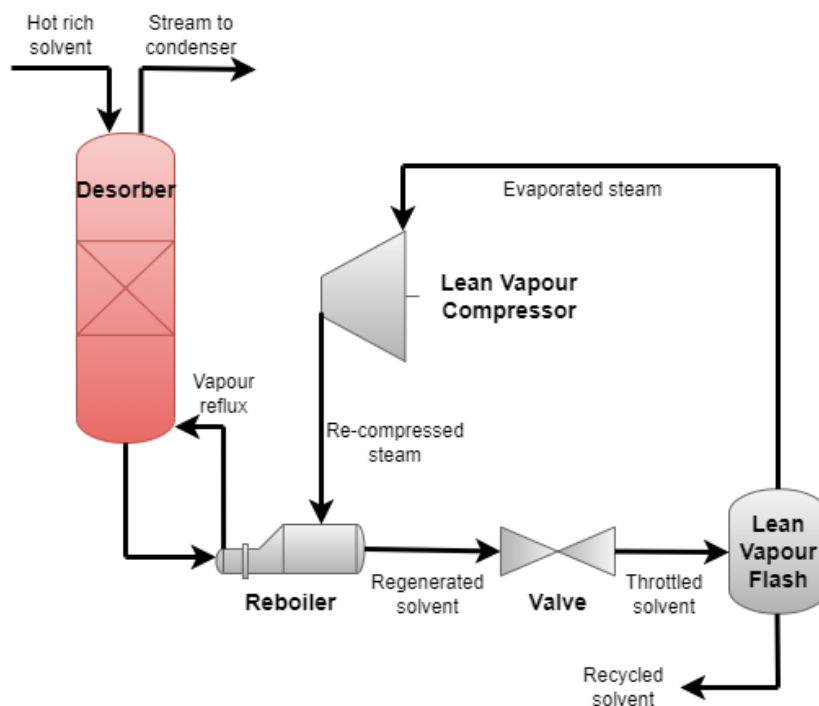


Figure 2.5: General scheme of lean vapour compression.

2.2.3.3 Intercooled Absorption (ICA)

The absorption of CO_2 is an exothermic reaction, giving rise to a temperature increase in the absorber. By applying cooling at an inter stage, so called intercooled absorption (ICA), the CO_2 reaction kinetics in the absorber is favoured. ICA is an absorber modification that extracts all or a part of the liquid flow on a stage, cooling it, to then recirculate it back to the absorber on the same stage. This makes it possible to control the temperature in the absorber while increasing the loading capacity of the solvent. An increased loading capacity results in a reduced solvent flow need, which could result in a lower reboiler duty [20]. This process modification will be investigated for the amine capture technology due to its atmospheric absorption column. Figure 2.6 illustrates a general schematic of an ICA.

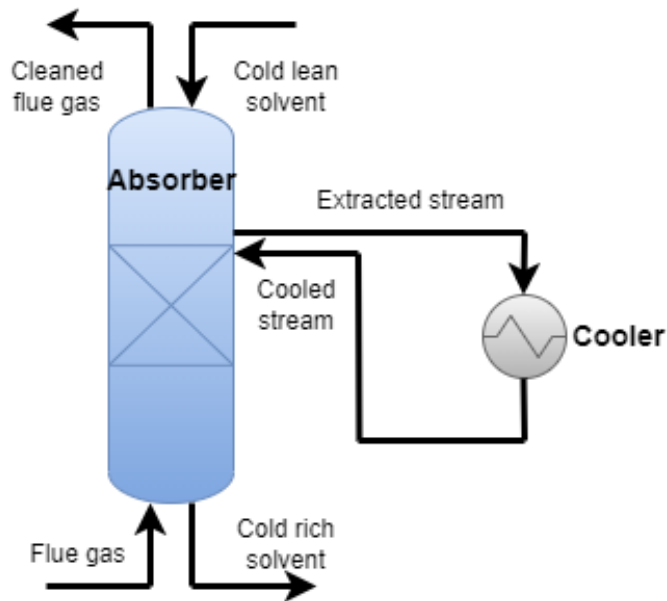


Figure 2.6: General scheme of intercooled absorption.

2.2.4 Liquefaction and Purification of CO₂

After the CO₂ has been captured from the flue gas stream it needs to be transported to the storage location. Since the storage locations mainly are at sea it requires relatively long distance transports from the capture locations to the storage locations. In order to conduct an efficient transportation system the CO₂ needs to be liquefied to allow for as much CO₂ to be transported as possible [26].

Also, the CO₂ needs to be in liquid state for the injection into porous rock formations, which is another reason for the requirement of the liquefaction process. However, the process of compressing a gas into a liquid is quite energy demanding, which makes it important to carry out the procedure in an efficient manner. In some cases the energy demand of the liquefaction stands for 10% of the total duty in the entire CCS process. In order to minimize the energy demand it is important to purify the CO₂ gas stream from water and other trace compounds such as SO_x and NO_x. The removal of water is also important to avoid formation of ice. The purification itself can however also be energy demanding, which makes it a trade-off matter when it comes to the degree of purification [26].

A general and simplified way to describe the liquefaction process is to describe it as a multistage compression with flashing prior to each stage and cooling subsequent to each stage. After the separated CO₂ gas stream leaves the desorber it enters a flash drum to separate water from the stream. Then the partly dewatered stream enters a compressor which increases the pressure of the stream. The compression also results in an increased temperature. Therefore the stream needs cooling, which leads to liquefaction of another portion of water in the stream. Afterwards the stream enters yet another flash drum to separate the liquefied water and this process gets repeated in multiple stages until there are negligible amounts of water and other trace compounds left, and the CO₂ reaches its liquid state [26].

In Figure 2.7, the correlating pressures and temperatures for liquefaction of CO₂ can be observed where the saturation line corresponds to the interface between vapour phase and liquid phase. Factors such as the composition of the CO₂ stream and the desired final pressure of the liquefied product play a major role in determining the most cost-effective liquefaction [27].

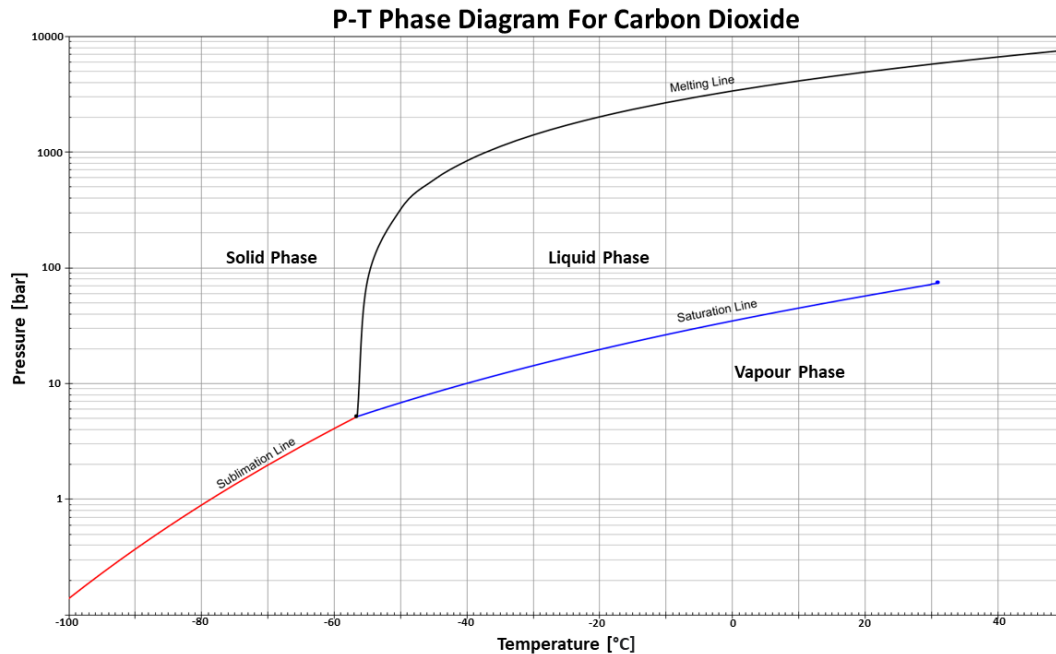


Figure 2.7: Pressure-temperature phase diagram for CO₂.

In the industry there are uncertainties regarding the cost-optimal pressure of the liquefied CO₂ for long distance transportation. Food grade CO₂ usually gets transported at 15 bar and -30°C, but those conditions might not be optimal for transporting industrially captured CO₂. In the ongoing research various pressure levels are evaluated, more specifically pressures between 7-70 bar. At the lower end of the span, i.e the low pressure CO₂, the temperatures are lower, which requires more electrical energy for the cooling of the stream. However, to obtain higher pressure more electrical energy is required for the compressors, which eventually makes it a trade-off matter. Other factors, such as the purity of the CO₂ stream, are also of importance when it comes to determining the optimum P-T conditions for the CO₂ transportation [27]. Nonetheless, in this project the target is to compress the CO₂ to 16 bar and -28 °C at VEAB's request.

2.2.5 Geological Storage of CO₂

There are various types of geological storage formations, i.e carbon sinks, where the liquefied CO₂ could be stored. The storage media with the highest capacities are depleted hydrocarbon reservoirs and deep saline aquifers. Other media with considerable storage potential are organic-rich shales, basaltic rocks and un-mineable coal seams. The storage mechanisms vary to a certain extent between these different carbon sinks, but in general the principle is the same. The CO₂ gets compressed to a supercritical state, around 100 bar, before being injected into permeable carbonate rock formations. Due to CO₂ having lower density than the surrounding media there are buoyancy forces which lift the CO₂ upwards. However, the CO₂ gets trapped by non-permeable so-called caprocks [28].

The CO₂ that will be captured at VEAB's CHP plant will be transported to a suitable storage site. There are a number of different possible choices but an example of one of the more developed projects is "Northern Lights". In the "Northern Lights" project, the imported liquefied CO₂ gets intermediately stored at a terminal before being sent to the storage reservoir. The reservoir is located 2600 metres below the bottom of the North sea, where the CO₂ gets transported via a pipeline from the intermediate storage terminal. The first phase of the Northern Lights project is planned to be initiated in 2024 where the annual CO₂ storage capacity will be 1.5 million tonnes [29].

3

Methodology

To evaluate the performance of each CO₂ capture technology, process simulations in Aspen Plus were performed. The process simulations began by setting up the models, i.e. putting in necessary information to obtain realistic results. Then suitable property methods for the capture process and liquefaction were chosen, which is described in Section 3.1.1. Then, in Section 3.1.2, the corresponding flue gas stream for SV3 at full load and half load were calculated using data obtained from VEAB. In order to simulate the chemistry and reactions that occurs, kinetic constants and equilibrium coefficients were added to the Aspen Plus model. The chemistry setup is described in Section 3.1.3.

The section that followed, Section 3.2, describes the process modelling approach for the CO₂ capture models and the liquefaction model. To investigate the effect of different parameters, a base case for each capture technology was made based on full load flue gas conditions. With this base case, a parameter study was performed with the purpose to find the most optimal parameters. This parameter study approach is further described in Section 3.2.1 for HPC and Section 3.2.2 for MDEA/DEA. Note that the parameter study was performed with full load conditions since a larger flue gas flow is expected to affect the CHP plant to a higher extent due to the higher energy usage.

To then evaluate the actual effect of CO₂ capture implementation, a heat integration to the CHP plant was performed for the optimized model for both full load and half load. The approach for heat integration is described in more detail in Section 3.3.

3.1 Aspen Plus Model Setup

In this section, the setup of the Aspen Plus models is described in more detail.

3.1.1 Property Methods for Aspen Plus Simulations

In order to obtain more reliable simulation results appropriate property methods, i.e. thermodynamic models, had to be added to the Aspen Plus model. Different property methods predict the behaviour of the chemicals involved based on their physical properties, which makes it important to select a property method that is customized for that certain mixture of components [30]. Depending on which part of the process that was simulated, different property methods were selected.

Since both the simulated CO₂ capture technologies contained electrolyte solutions, the decision was made to use the electrolyte non-random two-liquid (ELECNRTL) property method. This model is the most appropriate to perform phase equilibrium calculations in systems with mixed solvent electrolytes, which made it a sensible choice to implement in that part of the process [31]. But for the CO₂ liquefaction simulations the Soave-Redlich-Kwong (SRK) equation of state property method was considered to be the most fitting. In previously performed studies, the SRK equation of state has appeared to be a good predictor of the phase behaviour of CO₂ mixtures at elevated pressure levels [26]. Since the liquefaction process occurs at high pressures and mainly contain CO₂ and H₂O it was considered to be a reasonable choice. For the heat pump simulations the REFPROP method was used since it is developed for refrigerants [32].

3.1.2 Flue Gas Data

Both of the CCS technologies in focus are post-combustion capture technologies, i.e. the CO₂ is captured from the flue gas stream. Thus, to simulate a realistic case, real flue gas data was obtained from VEAB. As described previously in Section 1.1, the idea is to implement BECCS on VEAB's SV3 block, while keeping their other block (SV2) as peak load boiler. SV2 will thus be used as a back-up to meet the DH demand. In Table 3.1, the unconverted flue gas data from SV3, provided by VEAB, is presented.

Table 3.1: Unconverted flue gas data from VEAB.

Property	Unit	Typical/Average	Operating Range
Flue gas flow	Nm ³ /hr	168 000	65 000 - 175000
Temperature	°C	45	40 - 50
Moisture content	vol%	9	7 - 13
CO ₂ content	vol% dry gas	15	13 - 16.5
O ₂ content	vol% dry gas	4.5	4 - 7.5
Dust	mg/Nm ³ dry@6% O ₂	2	0 - 10
SO ₂	mg/Nm ³ dry@6% O ₂	<1	<5
HCl	mg/Nm ³ dry@6% O ₂	<0.5	<5
HF	mg/Nm ³ dry@6% O ₂	<0.1	<1
NO	mg/Nm ³ dry@6% O ₂	40	10 - 100
N ₂ O	mg/Nm ³ dry@6% O ₂	1	0 - 15
NH ₃	mg/Nm ³ dry@6% O ₂	5	1 - 10
CO	mg/Nm ³ dry@6% O ₂	50	0 - 150

The typical/average column in Table 3.1 corresponds to full load, which is what the base case models were based on. But, the values in Table 3.1 had to be converted into values that could be put into Aspen Plus. Thus, the components with unit "mg/Nm³ dry@6%" had to be converted using the air factor in the following Equation (3.1) [33].

$$AF = \frac{21 - x \text{ vol}\% \text{ O}_2(\text{dry})}{21 - y \text{ vol}\% \text{ O}_2(\text{dry})} \quad (3.1)$$

In Equation 3.1 AF is the air factor, x is the vol% of O₂ before conversion and y is the vol% of O₂ after conversion.

After converting the values to adjust for the actual O₂ content, the average volume flows were converted to molar flows using the ideal gas law, Equation 3.2.

$$n = \frac{P \cdot V}{R \cdot T} \quad (3.2)$$

Since the volumetric flow was given in Nm³, atmospheric pressure and 273.15 K was used to convert it to molar flow.

The obtained molar flows, listed in Table 3.2, were then fed into the Aspen Plus base case models and the optimized models for the full load case. Note that the content of dust, SO₂, HCl and HF were ignored since they were considered to be of negligible amount.

To estimate the flue gas stream at half load, the molar flows for all but O₂ and N₂ were halved. According to VEAB, the oxygen concentration should be 6% at half load, thus air (21% O₂ + 79% N₂) was added to fit this demand. Table 3.2 contains the molar flow and molar fraction of the flue gas flow for half load.

Table 3.2: Flue gas data input into Aspen Plus for full load and half load.

Component	Full Load		Half Load	
	Molar Flow [mol/hr]	Molar Fraction	Molar Flow [mol/hr]	Molar Fraction
N ₂	5 490 101	0.73	3 120 313	0.74
CO ₂	1 023 112	0.14	511 556	0.12
H ₂ O	674 579	0.09	337 290	0.08
O ₂	306 943	0.04	253 220	0.06
CO	300	$4.0 \cdot 10^{-5}$	150	$3.6 \cdot 10^{-5}$
NO	224	$3.0 \cdot 10^{-5}$	108	$2.5 \cdot 10^{-5}$
NH ₃	49	$6.6 \cdot 10^{-5}$	25	$5.9 \cdot 10^{-6}$
N ₂ O	4	$5.1 \cdot 10^{-7}$	2	$4.5 \cdot 10^{-7}$
Total	7 495 304	1	4 222 664	1

3.1.3 Reactions

When modelling in Aspen Plus, reaction chemistry in the properties environment (global chemistry) and reactions in the simulation environment must be defined. The Aspen Plus commando "Elec Wizard" in the properties environment was used to define the global chemistry for both models. In the simulation environment, a reaction set was made to describe the chemistry occurring in the the absorption and desorption columns. These reactions and constants were obtained from Aspen Plus example models, which exist for both HPC and MDEA/DEA technologies. In order to calculate the equilibrium constant $\ln(K_{eq})$, the software uses Equation 3.3 in which the equilibrium coefficients are used. In order to calculate the reaction rates, the software uses Equation 3.4 in which the kinetic constants are used. In Sections 3.1.3.1 and 3.1.3.2 the reactions as well as the used equilibrium coefficients and kinetic constants are tabulated.

$$\ln(K_{eq}) = A + \frac{B}{T} + C \cdot \ln(T) + D \cdot T \quad (3.3)$$

$$r = k \cdot \exp\left(-\frac{E}{R \cdot T}\right) \quad (3.4)$$

3.1.3.1 HPC Reactions

For HPC, three types of reactions were defined in the Aspen Plus model: equilibrium, kinetic and dissociation. Dissociation and equilibrium reactions were defined in the properties environment, corresponding to the global chemistry of the model. In the simulations environment, kinetic and equilibrium reactions were defined in reactions sets which were specified in the absorber and desorber blocks. Table 3.3 lists all the reactions that were registered in Aspen Plus. The equilibrium coefficients, corresponding to the equilibrium reactions in Table 3.3, are listed in Table 3.4. Similarly, the kinetic constants are presented in Table 3.5. The dissociation reactions do not need any constants since they correspond to ion dissociation, as a result of the HPC solvent being an ion solution.

Table 3.3: Reactions registered in Aspen Plus for absorption and desorption in the HPC cycle [34].

No.	Reaction Type	Stoichiometry
1	Equilibrium	$H_2O + HCO_3^- \rightleftharpoons CO_3^{2-} + H_3O^+$
2	Equilibrium	$2H_2O + CO_2 \rightleftharpoons HCO_3^- + H_3O^+$
3	Equilibrium	$2H_2O \rightleftharpoons OH^- + H_3O^+$
4	Kinetic	$CO_2 + OH^- \rightarrow HCO_3^-$
5	Kinetic	$HCO_3^- \rightarrow CO_2 + OH^-$
6	Dissociation	$KHCO_3 \rightarrow HCO_3^- + K^+$
7	Dissociation	$K_2CO_3 \rightarrow CO_3^{2-} + 2K^+$
8	Dissociation	$KOH \rightarrow OH^- + K^+$

Table 3.4: Equilibrium coefficients for Reactions 1-3 in Table 3.3 [34].

No.	A	B	C	D
1	216.1	-12 431.7	-35.5	0
2	231.5	-12 092.1	-36.8	0
3	132.9	-13 445.9	-22.5	0

Table 3.5: Kinetic constants for Reactions 4-5 in Table 3.3 [34].

No.	k	E [cal/mol]
4	$4.32 \cdot 10^{13}$	13 249
5	$2.38 \cdot 10^{17}$	29 451

3.1.3.2 MDEA/DEA Reactions

In the MDEA/DEA model, two types of reactions were defined: equilibrium and kinetic. As for HPC, kinetic and equilibrium reactions were defined in a reaction set in the simulation environment. Since MDEA/DEA is not a salt, the model does not have any dissociation reactions. Hence, only equilibrium reactions were defined as global chemistry in the properties environment. Table 3.6 illustrates the kinetic and equilibrium reactions and Table 3.7 and 3.8 lists their respective constants and coefficients.

Table 3.6: Reactions registered in Aspen Plus for absorption and desorption in the MDEA/DEA cycle [35].

No.	Reaction Type	Stoichiometry
1	Equilibrium	$2H_2O \rightleftharpoons OH^- + H_3O^+$
2	Equilibrium	$2H_2O + CO_2 \rightleftharpoons HCO_3^- + H_3O^+$
3	Equilibrium	$HCO_3^- + H_2O \rightleftharpoons CO_3^{2-} + H_3O^+$
4	Equilibrium	$DEAH^+ + H_2O \rightleftharpoons DEA + H_3O^+$
5	Equilibrium	$DEACOO^- + H_2O \rightleftharpoons DEA + HCO_3^-$
6	Equilibrium	$MDEAH^+ + H_2O \rightleftharpoons MDEA + H_3O^+$
7	Kinetic	$CO_2 + OH^- \rightarrow H_3O^+$
8	Kinetic	$HCO_3^- \rightarrow CO_2 + OH^-$
9	Kinetic	$DEA + CO_2 + H_2O \rightarrow DEACOO^- + H_3O^+$
10	Kinetic	$DEACOO^- + H_3O^+ \rightarrow DEA + CO_2 + H_2O$
11	Kinetic	$MDEA + CO_2 + H_2O \rightarrow MDEAH^+ + HCO_3^-$
12	Kinetic	$MDEAH^+ + HCO_3^- \rightarrow MDEA + CO_2 + H_2O$

Table 3.7: Equilibrium coefficients for Reactions 1-6 in Table 3.6 [35].

No.	A	B	C	D
1	132.9	-13 445.9	-22.5	0
2	231.5	-12 092.1	-36.8	0
3	216.1	-12 431.7	-35.5	0
4	-13.3	-4 218.7	0	9.9 e-3
5	16.5	-4 068.8	-1.5	0
6	-9.4	-4 235.0	0	0

Table 3.8: Kinetic constants for Reactions 7-12 in Table 3.6 [35].

No.	k	E [cal/mol]
7	$4.32 \cdot 10^{13}$	13 149
8	$2.38 \cdot 10^{17}$	29 451
9	$6.48 \cdot 10^6$	5 072
10	$1.34 \cdot 10^{17}$	11 497
11	$3.12 \cdot 10^8$	7 432
12	$1.26 \cdot 10^{12}$	15 334

3.1.4 Column Model Setup

When both the HPC and MDEA/DEA model were created some base settings were applied. In the properties environment in Aspen Plus all relevant components were specified. Then the chemistry was defined in both the properties and simulation environments, as previously described in Section 2.2.2.1. Then, both the absorber and desorber were created as RadFrac columns with the rate-based calculation type, due to its better accuracy compared to using the equilibrium calculation type [36]. To improve the possibility to get a converging solution the "Strongly non-ideal liquid" convergence model was used.

For the base model setup as well as for the parameter studies the column diameters were deliberately oversized for both consistency and convergence purposes. A column diameter of 10 meters gave a low approach to jet flood, hence it could be assumed that this diameter made the column oversized. To calculate the required amount of make-up solvent for each case, the "Balancer" command was used. In Table 3.9 the specified column settings are presented for both models.

Table 3.9: Column settings for base case model setup.

Column Configuration Settings	
Calculation Type	<i>Rate-Based</i>
Number of Stages (Amine Model)	<i>20</i>
Number of Stages (HPC Model)	<i>25</i>
Condenser	<i>None (both columns)</i>
Reboiler	<i>Kettle (only desorber)</i>
Operating Specifications	<i>Reboiler duty (only desorber)</i>
Valid Phases	<i>Vapor-Liquid</i>
Convergence	<i>Strongly non-ideal liquid</i>
Column Internals Settings	
Column Heights (Amine Model)	<i>20 m</i>
Column Heights (HPC Model)	<i>25 m</i>
Column Diameters (Both Models)	<i>10 m</i>
Mode	<i>Rating</i>
Internal Type	<i>Packing</i>
Packing Type	<i>Mellapak Sulzer Standard 250X</i>
Rate-Based Modeling Settings	
Flow Model	<i>Mixed</i>
Film Resistance (Liquid)	<i>Discretize Film (5 Discretization Points)</i>
Film Resistance (Vapour)	<i>Film Reactions</i>
Mass Transfer Coefficient Method	<i>Brf-85</i>
Heat Transfer Coefficient Method	<i>Chilton and Colburn</i>
Interfacial Area Method	<i>Brf-85</i>

Note that no condenser was specified in the desorber column. It was instead modeled as a cooler and flash drum which are separated from the column in order to obtain convergence easier. Also, for all compressors, turbines and pumps an 85% isentropic efficiency was assumed.

3.2 Process Modelling

In order to obtain a 90% CO₂ capture rate two design specifications were implemented in the models. The first design specification was set so the absorber captured 90% of the CO₂ in the flue gas by automatically manipulating the lean solvent flow rate. The second design specification was set so that a certain CO₂ loading was obtained in the regenerated solvent stream by manipulating the reboiler duty in the desorber. These design specifications made it possible to obtain 90% capture while finding the lowest reboiler duty for a specific loading. When both the design specifications were activated, the simulation was called a "locked model". When only the lean loading design specification was activated, the simulation was called a "semi-locked model". The following text describes how the specific heat duty, loading and capture rate were calculated and used during the process modelling.

The energy penalty for the regeneration of solvent was an important factor to track when modelling these technologies. To compare the performance of different models and cases regarding the energy penalty, the specific heat duty was used. The specific heat duty is universal since it considers not only the heat duty but also the captured CO₂. The specific heat duty was calculated according to Equation 3.5.

$$Q_{Spec} = \frac{Q_{Reb}}{M_{CO_2}} \quad (3.5)$$

Q_{Spec} is the specific heat duty (MJ/kgCO₂), Q_{Reb} is the reboiler duty for the desorber (MJ/hr), M_{CO_2} is the mass flow of CO₂ released in the desorber (kg/hr).

Throughout the modelling and the thesis, the term "loading" had a certain focus. Loading is defined as the molar ratio of apparent absorbed CO₂ and the amount of apparent solvent in the same stream. The term lean loading corresponds to the loading in the lean regenerated solvent that exits the desorber, and the rich loading is the loading in the rich stream that exits the absorber. The loading is defined as the ratio of the molar fraction of CO₂ derived components and the solvent derived components, which can be observed in Equations 3.6 and 3.7.

$$HPC \text{ Loading} = \frac{x_{CO_2}}{x_{K_2CO_3}} \quad (3.6)$$

$$MDEA/DEA \text{ Loading} = \frac{x_{CO_2}}{x_{MDEA} + x_{DEA}} \quad (3.7)$$

Two other important parameters when simulating the capture processes are the CO₂ capture rate and the absorber efficiency. The capture rate is defined as the ratio of captured CO₂ that gets sent to liquefaction, and the amount of CO₂ in the flue gas entering the absorber. The equation for calculating CO₂ capture rate can be seen in Equation 3.8.

$$CO_2 \text{ Capture Rate} = \frac{M_{CO_2 \text{ Captured}}}{M_{CO_2 \text{ Flue Gas}}} \quad (3.8)$$

The absorber efficiency is defined as ratio of the amount of CO₂ that gets absorbed in the absorber and the total amount of CO₂ in the flue gas that enters the absorber, which can be seen in Equation 3.9.

$$\text{Absorption Efficiency} = 1 - \frac{M_{CO_2 \text{ Absorber Loss}}}{M_{CO_2 \text{ Flue Gas}}} \quad (3.9)$$

Since the models are closed with a recirculation stream, the only loss of CO₂ occurs in the outlet gas flow from the absorber. This means that the CO₂ capture rate will always be the same as the absorber efficiency. This tendency is used in the design specifications to obtain the wanted capture rate during simulations, as described earlier in the section. However, the capture rate and the absorber efficiency are defined differently in this report to distinguish between the case when the absorber is in focus and the case when the whole system is in focus.

3.2.1 HPC Model

To begin with, a base case model was made in order to get the simulation started. The base case model was built as explained in Section 3.1 with one addition. By request from VEAB, pumps were added to account for the pressure drop associated to elevation differences between the columns. In Table 3.10 the base case model settings are presented and in Table 3.11 results of relevant variables are presented. The settings that were used for the base case model were chosen based on literature. A picture of the base case model can be seen in Figure 3.1.

After a converged base case model was obtained, a parameter study was performed to identify which parameters that could be changed to improve the model. The parameters that were evaluated for the HPC model were the absorber pressure, desorber pressure, absorber inlet temperature, lean solvent loading, HPC concentration in the lean solvent, liquid to gas (L/G) ratio in the absorber and the implementation of lean vapour compression (LVC). By starting from the base case model, one parameter was evaluated at the time which made it possible to see the effects of the specific model variable. As previously described in Section 3.2, the model contained the two design specifications, which led to denoting it as a locked model. However, when evaluating the L/G ratio only the lean loading design specification was used, hence it was called a semi-locked model. The capture rate design specification manipulated the absorber L/G ratio to obtain the desired capture rate and was therefore inactivated in order to evaluate how different L/G ratios affected the process.

3.2.2 MDEA/DEA Model

Similarly to HPC, a base case model was made as a first step of the simulation. Also for MDEA/DEA, pumps were added to account for the pressure drop associated to the elevation difference between the columns. The base case model settings for MDEA/DEA are presented in Table 3.12 and the results are presented in Table 3.13. As for the HPC model, the settings that were used in the base case were based on literature. In Figure 3.2, the base case Aspen Plus model for MDEA/DEA is shown.

Like for the HPC model, a parameter study was performed to optimize the MDEA/DEA model performance. The evaluated parameters were the desorber pressure, the absorber inlet temperature, lean solvent loading, MDEA/DEA composition in lean solvent and L/G ratio in the absorber. In addition, the implementation of LVC and intercooled absorption (ICA) was evaluated. Also, the same design specifications as for the HPC model was used for the MDEA/DEA model.

Table 3.12: MDEA/DEA base case model settings.

Base Case Settings	
Absorber Pressure	1 atm
Desorber Pressure	1 atm
Lean Solvent Temperature	45°C
Lean Solvent Loading	0.03
MDEA Concentration	20wt%
DEA Concentration	20wt%

Table 3.13: MDEA/DEA base case model results.

Base Case Results	
L/G Ratio	5.32
Make-up	1.16%
Reboiler Duty	4.87 MW
Specific Heat Duty	4.32 MJ/kgCO ₂
HEX Duty	37.51 MW
Pump Duty	0.23 MW
Condenser Duty	12.78 MW
Cooler Duty	26.12 MW

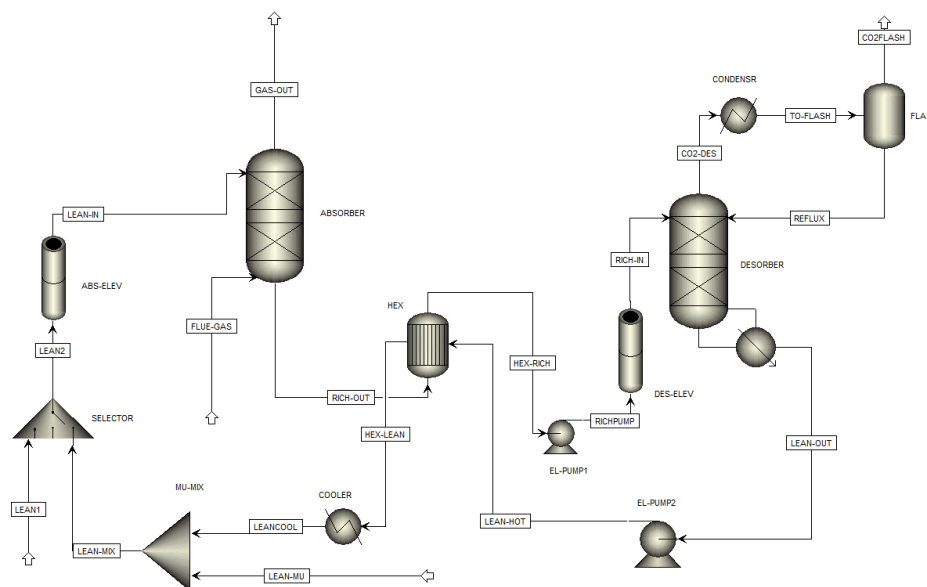


Figure 3.2: Aspen Plus MDEA/DEA base case model.

3.2.3 Liquefaction Model

The same liquefaction model was used for both HPC and MDEA/DEA but each case was simulated with their respective CO₂ capture stream. The CO₂ liquefaction model was built and simulated in accordance with the specifications in the article by Deng et al [27]. Hence, the liquefaction was carried out in the form of a three stage compression train and external cooling in the form of an ammonia heat pump.

First, the CO₂ was compressed to 27.5 bar with a constant pressure ratio over the compressors. After each compressor the stream was air cooled and liquefied water was separated. After the last compressor a "Separator" block was added to remove excess O₂, NH₃ and H₂O to meet relevant industry standards. Note that this is a simplification of reality and it was assumed that this operation did not require any energy. The CO₂ stream was then air cooled before being liquefied via heat exchanging with the external heat pump before entering a purge flash drum, to remove excess impurities. The stream was then expanded to 16 bar before entering the last flash drum where the liquid outlet was the desired product. The vapour stream consisting of mostly CO₂ was re-compressed and recycled back to the stream that entered the liquefaction heat exchanger. The Aspen Plus model for liquefaction can be seen in Appendix A.

The pressures and temperatures in the ammonia heat pump were specified in a way that it could both cool the CO₂ stream and recover excess heat to the district heating network. The flow rate of ammonia was adjusted so it would meet the required duty in the heat exchanger with the CO₂ stream.

3.3 Heat Integration

After the parameter studies of the carbon capture models were completed, the models were optimized based on the results from the parameter studies. Two simulations of the optimized models for each technology were made, one for full load and one for half load. Then, based on the results from these optimized models, a heat integration to VEAB's SV3 was performed. Equation 3.10 below was used to calculate the sizes of the district heating (DH) water streams to meet the cooling demands of the carbon capture process streams and reaching 95 °C. It was assumed that the DH water entered the heat exchanger at 45 °C and had a constant specific heat capacity of 4.18 kJ/kgK. Regarding ΔT_{min} for different types of heat exchangers it was assumed 15 K for gas-gas, 10 K for gas-liquid and 5 K for liquid-liquid.

$$\dot{m}_{DHwater} = \frac{Q}{C_{P,water} \cdot \Delta T_{DHwater}} \quad (3.10)$$

In Equation 3.10 $\dot{m}_{DHwater}$ is the massflow of DH water in kg/s, Q is the heat exchanger duty in J/s, $C_{P,water}$ is the specific heat duty for water in J/kgK and $\Delta T_{DHwater}$ is the temperature difference of the inlet and outlet DH stream in the unit K.

The following sections will describe the heat integration approaches that were made for HPC, MDEA/DEA and liquefaction in more detail.

3.3.1 HPC

The HPC model was primarily optimized to minimize the reboiler duty and the compression demand. However, one setting was kept constant in order to benefit the heat integration. By flashing the liquid outlet stream from the desorber at 0.59 bar it resulted in the stream cooling down to 90 °C, which was the specified absorber inlet temperature. Hence, no heat exchanger was needed to cool down the stream before entering the absorber. Thus, keeping the pressure in the flash constant at 0.59 bar resulted in two, rather than three cooling operations in the entire HPC process. One being the desorber condenser and the other being the pressurized flue gas cooler. Both streams had sufficiently high temperatures for directly warming the DH water to 95 °C. By using Equation 3.10, the amount of heated DH water could be calculated.

3.3.2 MDEA/DEA

The streams in the amine cycle that needed external cooling were too cold to directly heat DH water to 95 °C. Hence, heat pumps were simulated in Aspen Plus to transport heat from the MDEA/DEA capture process streams to the DH network, at the cost of compression work input. The heat from the desorber condenser was used to preheat DH water. The rest of the required heat, to reach 95 °C for the DH water, was provided by a heat pump that was connected to the absorber inlet cooler. However, there was still a large amount of excess heat in the absorber inlet stream which was used to directly heat DH water via a parallel heat pump condenser. This heat pump, that uses the excess heat in the absorber inlet cooler to heat DH water, is called "Heat Pump 1" (HP1). But there was also another heat pump that was simulated to cool down the absorber intercooling stream while heating DH water, called "Heat Pump 2" (HP2). The amount of DH water required to meet the condenser duties was calculated using Equation 3.10, with the same DH-assumptions as stated in Section 3.3. Appendix B contains pictures of the simulated heat pumps and a table listing the evaporator, condenser and power duties for HP1 and HP2.

3.3.3 Liquefaction

In the CO₂ compression train the post compression coolers were assumed to be air coolers, since the duties were considered to be insufficient for being integrated to the DH system. However, the ammonia heat pump was designed so that the heat from the condenser could be integrated to the DH system. The amount of DH water required to meet the condenser duty was calculated using Equation 3.10, with the same assumptions as in Section 3.3.

4

Parameter Study & Model Optimization

After the base case carbon capture models had been developed in Aspen Plus it was time for optimizing the models in order to minimize the energy penalty as well as the electricity demand. The models were also optimized with respect to the heat integration to maximize the energy recovery. To find the optimal settings for respective model several parameter studies were performed which can be seen in the following sections. In the parameter studies, one parameter was changed at a time to investigate how a change in that parameter affected the energy and power demand. The results from the parameter studies are then used to create the final optimized models for HPC and MDEA/DEA. Also, the optimized models were simulated for a half load case where the flue gas input is decreased to the values presented in Table 3.2.

4.1 HPC Parameter Study

In the following sections, the results from the HPC model parameter study are presented.

4.1.1 Absorber Pressure

In the base case model the absorber was operated at a pressure of 7 bar. In the parameter study the pressure was varied between 6-10 bar to evaluate how it affected the reboiler duty, the compander duty and the L/G ratio. In Figures 4.1, 4.2 and 4.3 it is presented how the absorber operating pressure affected these variables.

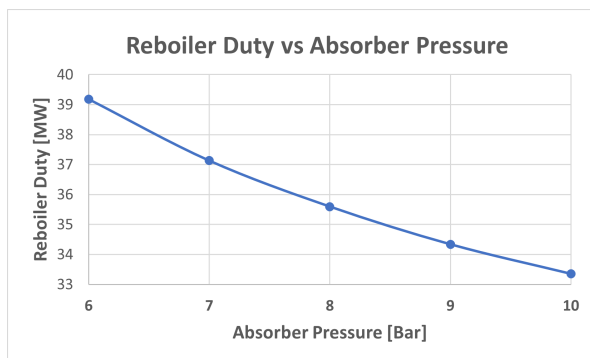


Figure 4.1: Reboiler duty as a function of absorber pressure.

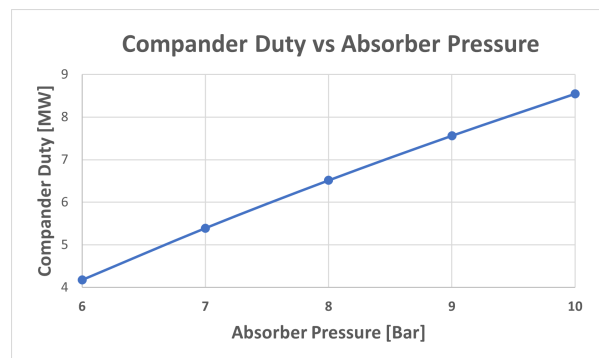


Figure 4.2: Compander net duty as a function of absorber pressure.

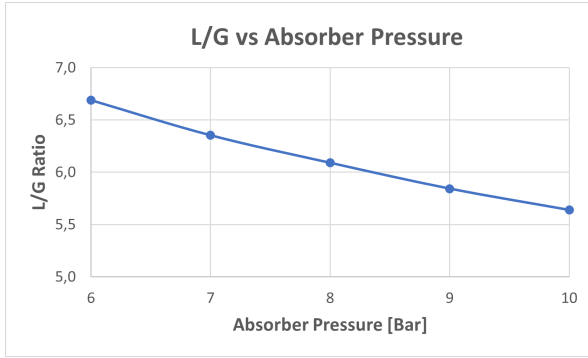


Figure 4.3: L/G ratio as a function of absorber pressure.

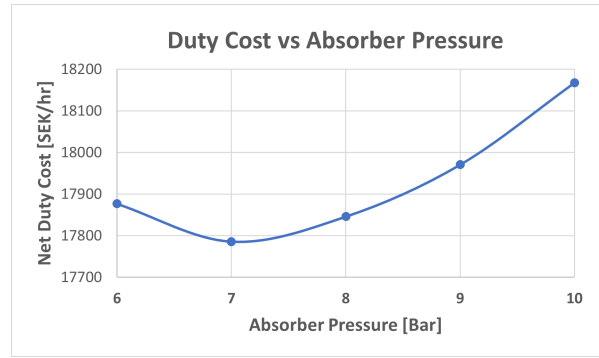


Figure 4.4: Net duty cost as a function of absorber pressure.

Figure 4.3 shows that an increased pressure allows for better absorption, leading to a smaller flow rate of lean solvent required to meet the capture rate design specification. A smaller volume of solvent in the system leads to a smaller energy demand to regenerate it, which can be seen in Figure 4.1. However, an increased absorber operating pressure requires a higher compression demand of the flue gas, which can be seen in Figure 4.2, as well as a higher pumping duty of the regenerated solvent. Nonetheless, pumping a liquid is significantly less energy demanding compared to compressing a gas, leading to the change in pumping duty being considered negligible in this case. In Figure 4.4 it can be seen that 7 bar is the cost-optimum pressure to operate the absorber based on the assumption of a steam price of 400 SEK/MWhr and an electricity price of 600 SEK/MWhr (specified values from VEAB). However, it is important to note that the optimal pressure is sensitive to changes in steam price as well as electricity price. An increased electricity price would shift the optimum to a lower pressure and vice versa for a case where the steam price increases.

4.1.2 Desorber Pressure

Initially in the base case the desorber was operated at atmospheric pressure. In Figure 4.5 the specific heat duty is plotted against the desorber pressure in the range from 1.01 to 2 bar.

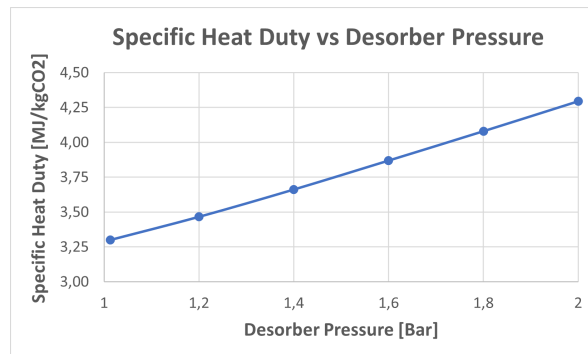


Figure 4.5: Specific heat duty as a function of desorber pressure.

From the plot in Figure 4.5 it can be seen that the specific heat duty increases with increasing desorber pressure. From these results it can be concluded that a lower pressure benefits the CO₂ desorption process, which is in line with the literature regarding a pressure swing cycle. However, a higher pressure of the CO₂ exiting the column would lead to a lower compression demand and thereby a lower electricity consumption in the liquefaction process. As mentioned in Section 4.1.1, the cost-optimum conditions are sensitive to duty price fluctuations. A higher electricity price would shift the optimum to a higher temperature and vice versa for a higher steam price.

4.1.3 Absorber Inlet Temperature

In the base case model the absorber was operated at a temperature of 90 °C. In the parameter study the temperature was varied between 85-105 °C to evaluate how it affected the reboiler duty, the compander duty and the L/G ratio. In Figures 4.6, 4.7 and 4.8 it is presented how the absorber operating temperature affected these variables.

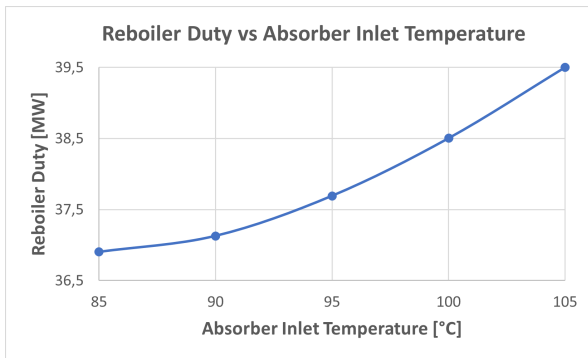


Figure 4.6: Reboiler duty as a function of absorber temperature.

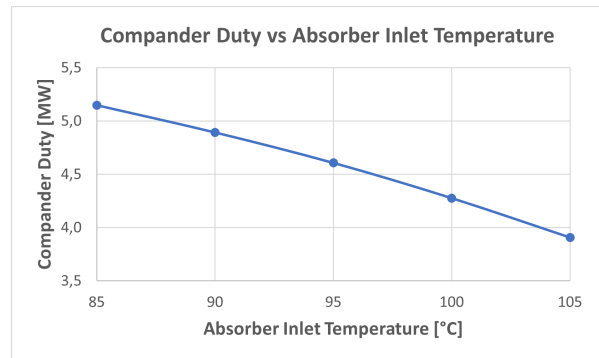


Figure 4.7: Compander net duty as a function of absorber temperature.

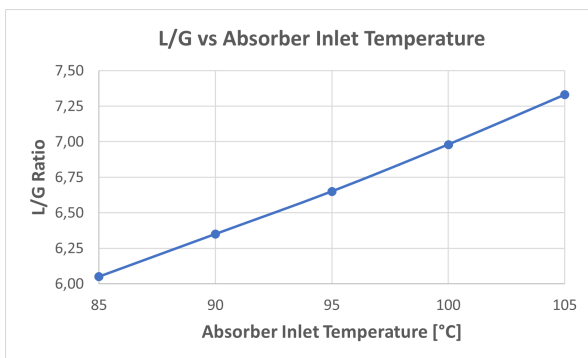


Figure 4.8: L/G ratio as a function of absorber temperature.

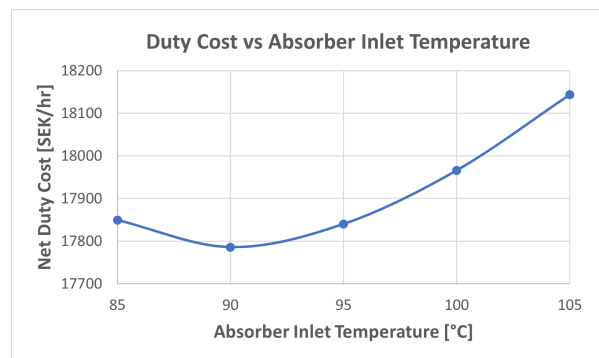


Figure 4.9: Net duty cost as a function of absorber temperature.

Compared to results in section 4.1.1 the inverse trends can be seen by increasing the inlet temperature. This is due to the absorption being favoured by lower temperatures, meaning an increased temperature would require an increased flow rate of lean solvent to meet the capture rate design specification, which leads to a higher reboiler duty.

However, a higher temperature correlates to more energy being stored in the streams, which leads to more electricity being generated in the expander, resulting in a net decrease of the compander duty. In Figure 4.9 it can be seen that 90 °C is the cost-optimum temperature to operate the absorber based on the assumption of a steam price of 400 SEK/MWhr and an electricity price of 600 SEK/MWhr.

4.1.4 Lean Solvent Loading

A lean solvent loading of 0.3 was specified in the design specification in the base case simulation. In this parameter study the lean solvent loading was varied between 0.25-0.35 to see how it affected the specific heat duty and the L/G ratio, which can be observed in Figures 4.10 and 4.11.

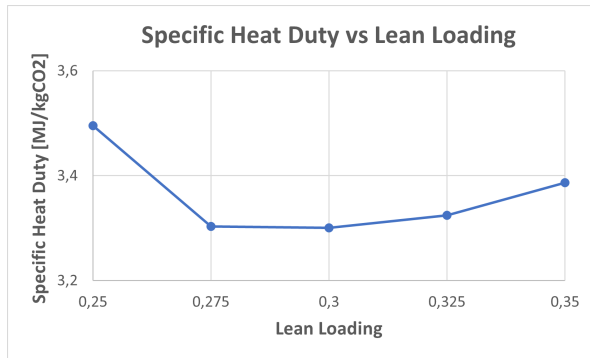


Figure 4.10: Specific heat duty as a function of lean solvent loading.

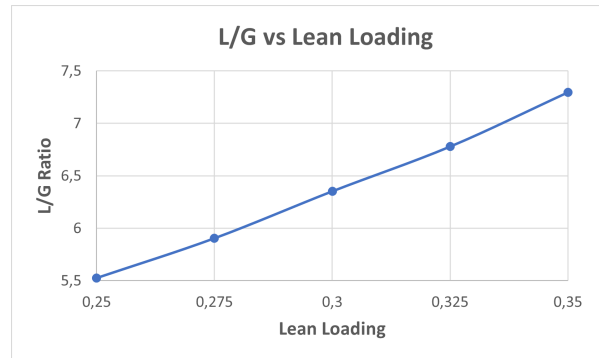


Figure 4.11: L/G ratio as a function of lean solvent loading.

In Figure 4.10 it can be seen that there is an optimum lean loading at 0.3 with regards to the specific heat duty even though that the L/G ratio keeps increasing, which can be seen in Figure 4.11. The increasing L/G ratio could be due to more solvent being required to match the 90% absorber efficiency when the loading is higher. A higher loading corresponds to a larger apparent CO₂ flow in the regenerated solvent stream, which pushes the equilibrium and diminishing the CO₂ absorption kinetics. Hence, more solvent is required to absorb 90% of the CO₂ coming from the flue gas. The reason that the specific heat duty does not follow the same trend could be due to the dependence on more factors than just the absorber efficiency. A lower loading would lead to less liquid passing through the reboiler corresponding to a lower energy penalty. However, in order to reach a lower loading in the regenerated solvent more CO₂ needs to be released, requiring a larger energy input. At the other end of the spectrum, a higher loading leads to less energy needed to release CO₂, but a larger liquid flow through the reboiler. Hence, it is a trade-off matter and an optimum loading with regards to the energy penalty can be found somewhere in the middle as seen in Figure 4.10.

4.1.5 Lean Solvent K_2CO_3 Concentration

The concentration of K_2CO_3 in the lean solvent in the base case model was 25 wt%. In the parameter study the K_2CO_3 concentration in the lean solvent was varied between 20-40 wt% to see the effect on the specific heat duty, which can be seen in Figure 4.12.

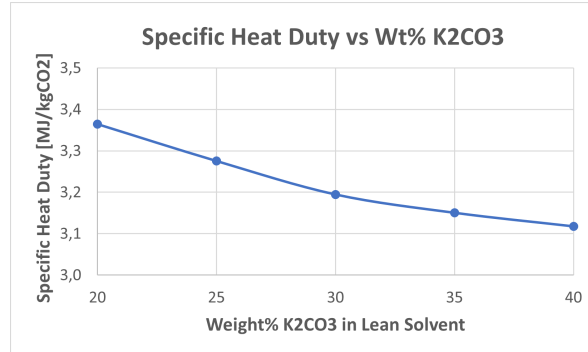


Figure 4.12: Specific heat duty as a function of lean solvent K_2CO_3 concentration.

From Figure 4.12 it can be seen that the higher concentration of K_2CO_3 in the solvent, the lower the energy penalty. This could be due to a lower L/G being required for a solvent with a higher concentration, meaning less liquid passing through the reboiler. However, due to risk of salt precipitation damaging the equipment at higher concentrations, the optimal concentration is considered to be 30 wt% [37]. This would be a compromise between minimized risk of precipitation and minimized energy penalty.

4.1.6 L/G Ratio (Semi-Locked)

The locked base case model contained an absorber design specification that optimized the L/G ratio to meet 90% capture rate. But, as stated in Section 3.2, to evaluate how the L/G affected the absorber efficiency the design specification was deactivated, thus creating a semi-locked model. In Figure 4.13 the absorber efficiency is presented as a function of the L/G ratio.

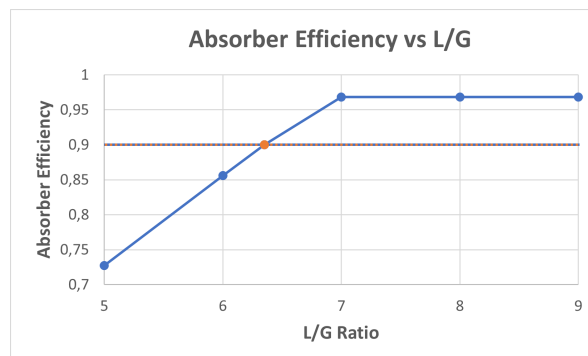


Figure 4.13: Absorber efficiency as a function of the L/G ratio.

In Figure 4.13 it can be observed how the absorber efficiency relatively linearly increases with an increased L/G ratio until it reaches an upper limit of how much CO_2 can be absorbed.

4.1.7 Lean Vapour Compression (Atmospheric LV-Flash)

The lean vapour compression was simulated at various lean vapour pressures while varying the desorber pressure, which can be seen in Figures 4.14 and 4.15.

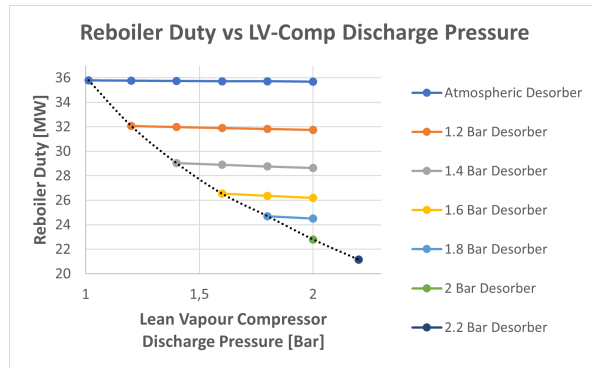


Figure 4.14: Reboiler duty as a function of lean vapour compressor discharge pressure.

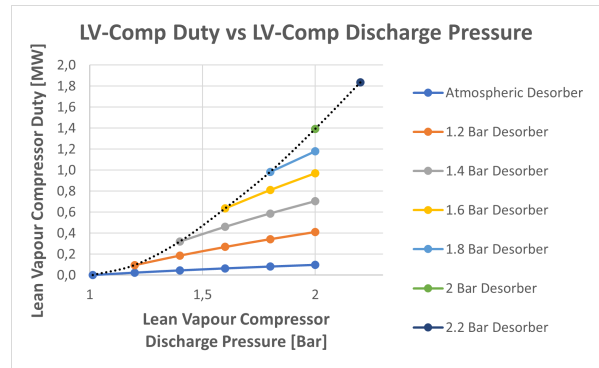


Figure 4.15: Lean vapour compressor duty as a function of discharge pressure.

From the series in Figure 4.14 it can be seen that the reboiler duty barely changes when increasing the lean vapour pressure while having the desorber pressure constant. This proves that it is not feasible to compress the lean vapour to any pressure above the desorber pressure, since it requires more compression duty and has a negligible effect on the reboiler duty. Hence, only the first data points in each series are of interest, where the lean vapour pressure is the same as the reboiler pressure. The dotted lines in both figures above are indicating how the duties change with an increasing LVC pressure.

It is also worth noting that the reboiler duty decreases with an increasing desorber pressure, which is opposite of the base case model in section 4.1.2. This is due to that a higher desorber pressure allows for more steam to be recycled within the system as well as some electricity being put into the system leading to a lower reboiler duty. However, there is an optimum between the operating cost and the desorber pressure, which is further discussed in Section 4.1.8.

4.1.8 Lean Vapour Compression (Sub-atmospheric LV-Flash)

In order to adjust the model, to make the heat integration more efficient, the LV-flash was operated at 0.59 bar. As explained in Section 5.2, this led to the regenerated solvent reaching a temperature of 90 °C and thereby did not need any cooling before entering the absorber. The sub-atmospheric flashing also led to more vapour being recirculated to the reboiler, which led to a lower reboiler duty.

In this study the LVC pressure was evaluated to find the cost-optimum solution for the case when the LV-flash was operated at the pressure that diminished the need of cooling the regenerated solvent. In Figure 4.16 the combined duty cost for the reboiler and LV compressor is presented as a function of the LVC pressure. In order to calculate the cost it was assumed that the price for steam is 400 SEK/MWhr and 600 SEK/MWhr

for electricity. Note that the compander duty is not accounted for in this cost since it remained constant for all cases.

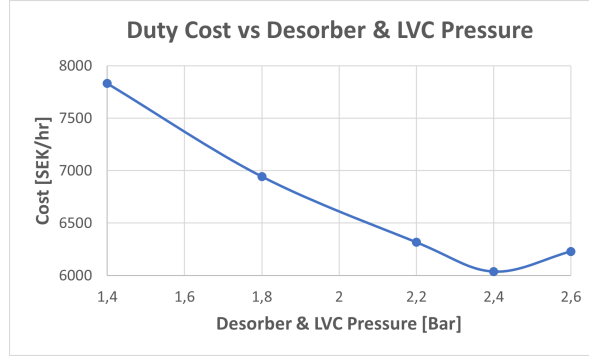


Figure 4.16: Duty cost as a function of LVC & desorber pressure.

As can be seen in Figure 4.16 the cost optimal LVC and desorber pressure was at 2.4 bar resulting in a duty cost of 6038 SEK/hr. As mentioned in previous sections, the cost-optimum conditions vary with varying duty prices. In this case, a higher electricity price would shift the cost-optimum to lower pressures and the other way around for a higher steam price.

4.1.9 Optimized HPC Model

As mentioned in section 4.1 the parameter studies were performed with oversized columns in order to facilitate convergence. This led to slightly skewed results in the parameter study, but the trends that were identified are considered to be valid. Thus, to get more realistic results for the optimized model, the column diameters were downsized to match 80% flood approach [38]. When downsizing the columns the net duty slightly increased resulting in a duty cost of 6636 SEK/hr, with the compander and pump duties excluded. Adding the compander and pump duties it results in a total duty cost of 10166 SEK/hr. This is the model that is being used for the heat integration to the CHP plant, which is further discussed in Section 5. In Tables 4.2 and 4.1 the final settings and results of the HPC model are presented. Note that the optimized model has LVC implemented and thereby some settings that seemed optimal in the parameter study, which was performed on the base case model without LVC, were not optimal for this model.

Table 4.1: HPC optimized downsized model settings.

Optimized Downsized Model Settings	
Absorber Diameter	4.03 meters
Desorber Diameter	3.83 meters
Column Heights	25 meters
Lean Solvent Loading	0.285
K ₂ CO ₃ Concentration	30 wt%
Absorber Pressure	7 Bar
Desorber & LVC Pressure	2.4 Bar
Absorber Inlet Temperature	90 °C

Table 4.2: HPC optimized downsized model results.

Optimized Downsized Model Results	Full Load	Half Load
L/G Ratio	5.46	4.96
Lean Solvent Make-up	0.36%	0.77%
Reboiler Duty	7.93 MW	3.66 MW
Specific Heat Duty	0.70 MJ/kgCO ₂	0.64 MJ/kgCO ₂
LVC Duty	5.77 MW	2.93 MW
Specific LVC Duty	0.51 MJ/kgCO ₂	0.51 MJ/kgCO ₂
Cooler 1 Duty	3.39 MW	1.70 MW
Cooler 2 Duty	-	-
Condenser Duty	12.94 MW	5.39 MW
Pump Duty	0.48 MW	0.24 MW
Compander Net Duty	5.64 MW	2.97 MW
Carbon Capture Duty Cost	10 166 SEK/hr	5 148 SEK/hr
Liquefaction Compression Duty	3.96 MW	2.41 MW
Liquefaction DH Recovery	4.57 MW	2.43 MW
Carbon Capture & Liquefaction Duty Cost	12 538 SEK/hr	6 588 SEK/hr

Comparing the results in Table 4.2 with the results from the base case in section 4.1, it can be concluded that the process modifications resulted in considerable decreases in external duty requirement. The specific heat duty decreased from 3.30 MJ/kgCO₂ to 0.7 MJ/kgCO₂, at the expense of an added electricity input. The specific heat duty for the base case model can be validated against literature values in Appendix D. However, it is important to note that it is not pure external energy duty minimization, since the optimized system has one cooler less that delivers heat to DH water. The heat is instead recirculated within the system by means of LVC and less heat is being recovered in the form of DH.

Apart from the duty minimization, an advantage with the optimized system is that the heat from the condenser can be used for district heating which is not the case for the base model due to insufficient temperatures. In order to utilize the heat in the incoming condenser stream in the base model, it would be needed to install a heat pump. Another advantage with the optimized model is that the CO₂ stream is delivered to the liquefaction process at an already elevated pressure, which reduces the compression demand downstream.

It can be concluded from Figure 4.18 that a higher desorber pressure corresponds to a lower specific heat duty. This is due to the fact that a higher column pressure results in a higher desorber temperature, thus driving the equilibrium to releasing CO_2 . Hence, since the pump duty related to the pressure increase is considerably low, it is beneficial to use the maximum 2 bar desorber pressure in the optimized model.

4.2.2 Lean Solvent Temperature

In the base case the lean solvent temperature was held at $45\text{ }^\circ\text{C}$, and in the parameter study the lean solvent temperature was varied between $60\text{ }^\circ\text{C}$ to $20\text{ }^\circ\text{C}$ to evaluate how it affected the model performance. Figure 4.19 illustrates how the temperature affects the specific heat duty while Figure 4.20 illustrates how it affects the L/G ratio. It is worth mentioning that a lean solvent temperature below $45\text{ }^\circ\text{C}$ could diminish the potential of heat integration to the CHP plant, thus $45\text{ }^\circ\text{C}$ was considered to be most appropriate temperature for the optimized model.

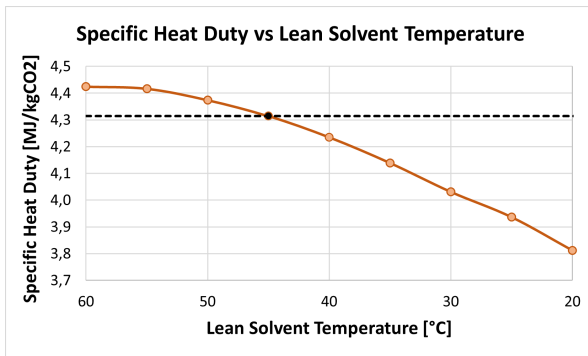


Figure 4.19: Specific heat duty as a function of lean in temperature to the absorber, with the black line represents the base case.

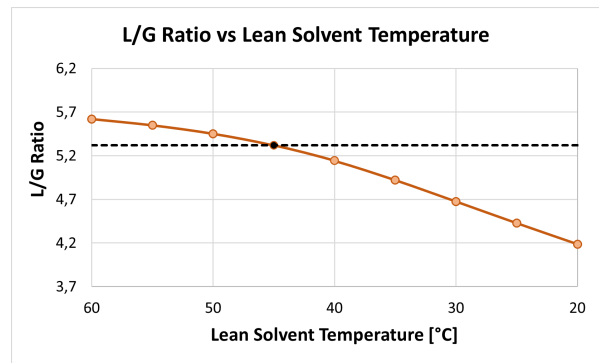


Figure 4.20: L/G Ratio as a function of lean in temperature to the absorber, with a black line represents the base case.

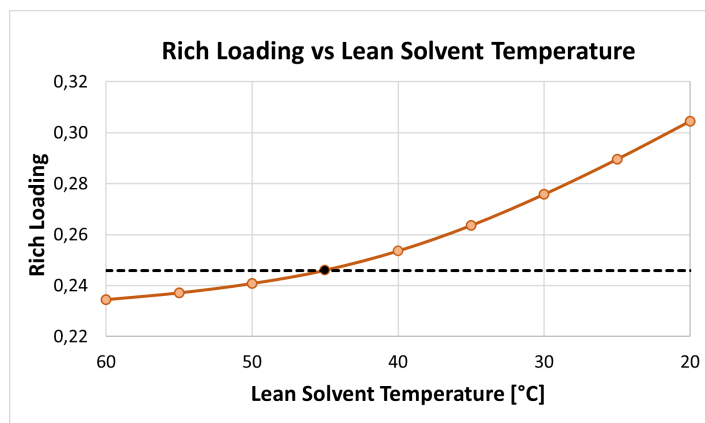


Figure 4.21: Rich loading as a function of lean in temperature to the absorber, with a black line represents the base case.

It is evident that a low lean solvent temperature is beneficial due to the decreasing specific heat duty trend in Figure 4.19. The reboiler duty decreases due to declining trend of the L/G ratio, seen in Figure 4.20. The L/G ratio decrease is a result of the increased rich loading, since that corresponds to a higher CO₂ concentration entering the desorber. These declining trends can be explained by noting that CO₂ absorption is favoured at lower temperatures, hence 90% absorption efficiency can be obtained at lower L/G resulting due to higher rich loading.

4.2.3 Lean Solvent Loading

The design specification for lean loading was set at 0.03 for the base case but to determine the most optimal value, the lean loading was varied between 0.01 and 0.05. The resulting specific heat duty and L/G ratio can be seen in Figure 4.22 and Figure 4.23 respectively.

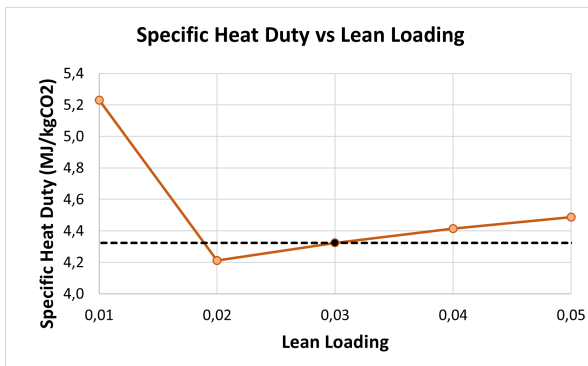


Figure 4.22: Specific heat duty as a function of lean solvent loading, with a black line represents the base case.

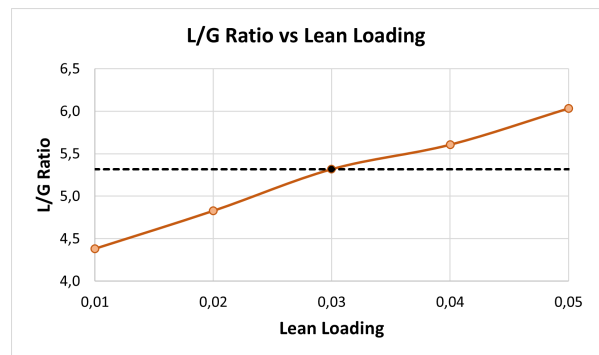


Figure 4.23: L/G Ratio as a function of lean solvent loading, with a black line represents the base case.

Figure 4.22 illustrates that it exists an optimum lean loading at 0.02, which corresponds to the lowest specific heat duty. As mentioned in section 4.1.4, the optimum lean loading might depend on a trade off between higher regeneration energy requirement for a low lean loading and a higher L/G ratio for a high lean loading.

4.2.4 Lean Solvent MDEA/DEA Composition

The lean solvent composition for the base case was 20 wt% MDEA and 20 wt% DEA and to make a representative parameter study, mixtures of a total 40 wt% MDEA/DEA were evaluated. Figure 4.24 illustrates how the specific heat duty varies for different mixtures of MDEA/DEA with respect to lean loading. Figure 4.25 is an enlarged view of the same plot, focused on the lower specific heat duties.

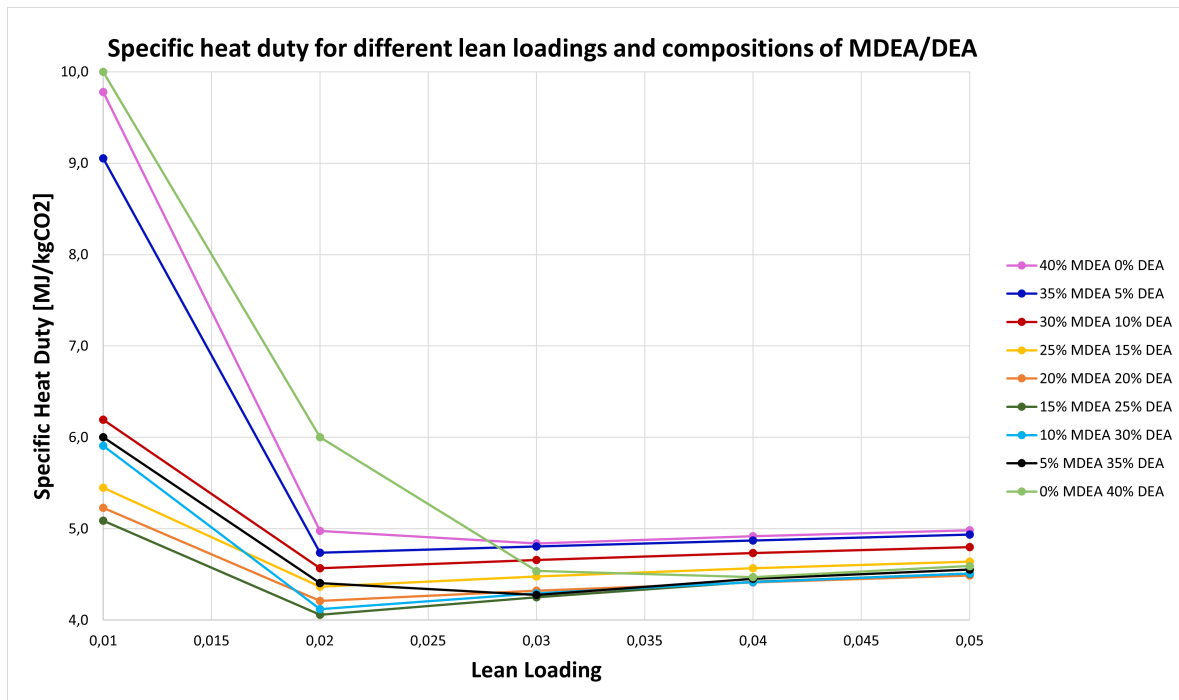


Figure 4.24: Specific heat duty as a function of lean loading for different MDEA/DEA mixtures.

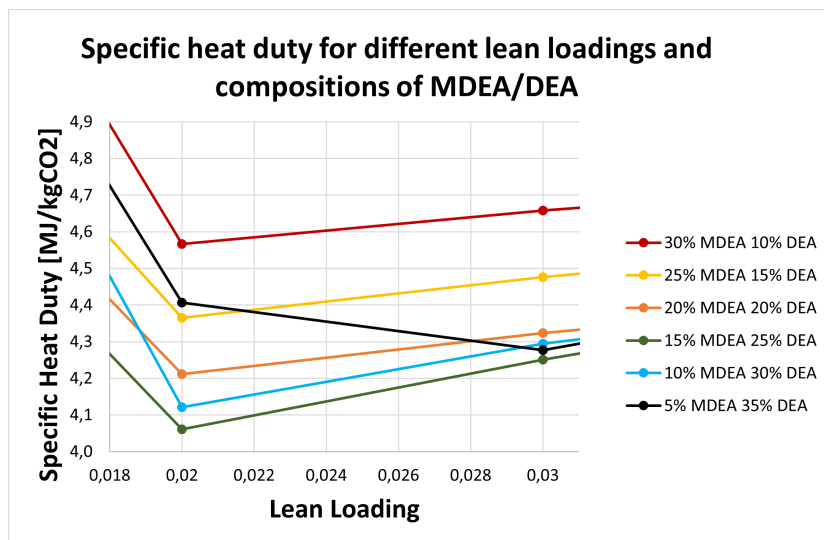


Figure 4.25: Specific heat duty as a function of lean loading for different MDEA/DEA mixtures, zoomed in.

From Figure 4.24 and Figure 4.25 it can be concluded that the optimum lean loading can vary for different MDEA/DEA blends. As one example, the mixture 5% MDEA and 35% DEA has an optimum lean loading at 0.03 whereas the mixture 30% MDEA and 10% DEA has an optimum at 0.02. Regarding the specific heat duty, more heterogeneous mixtures seem to be favoured due to their lower specific heat duty. Figure 4.25 illustrates that the mixture 15 wt% MDEA and 25 wt% DEA gave rise to the lowest energy consumption and is therefore the most optimal mixture.

4.2.5 L/G Ratio (Semi-Locked)

The base case was simulated as a locked model using a design specification to find the L/G ratio that meets 90% capture in the absorber. Figure 4.26 illustrates the results from varying the L/G ratio on a semi-locked model i.e. a model without that design specification.

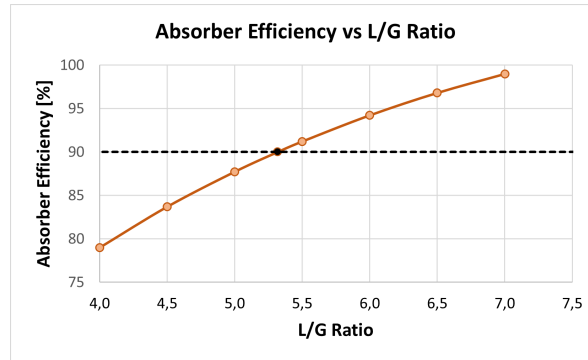


Figure 4.26: Absorber efficiency as a function of L/G Ratio, with a black line represents the base case.

Varying the L/G ratio on a semi-locked model showed a somewhat linear trend with respect to the absorber efficiency. This is reasonable since a lower L/G ratio results in less solvent entering the absorber and thereby the absorber efficiency decreases.

4.2.6 Lean Vapour Compression

For the MDEA/DEA capture technology three LV-flash pressures were investigated for three different desorber pressures. The three LV-flash pressures were 1.01 bar, 0.8 bar and 0.6 bar. The three desorber pressures were 1 atmosphere, 1.75 bar and 2 bar. Figure 4.27 illustrates how the specific heat duty is affected by LVC, Figure 4.28 shows how the specific LV compressor duty varies with LV-flash pressure and Figure 4.29 illustrates the total duty cost of implementing LVC. The duty cost was calculated using 400 SEK/MWhr for extracted steam and 600 SEK/MWhr for electricity, as explained in section 4.1.8.

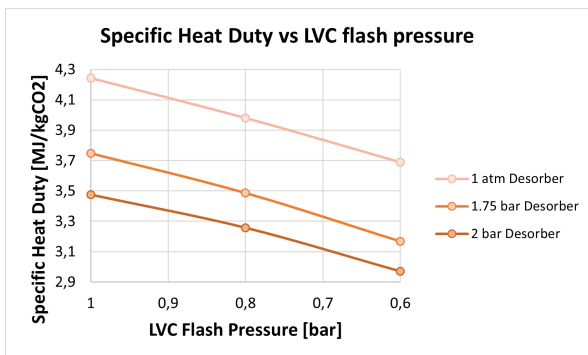


Figure 4.27: Specific heat duty as a function of LV-flash pressure.

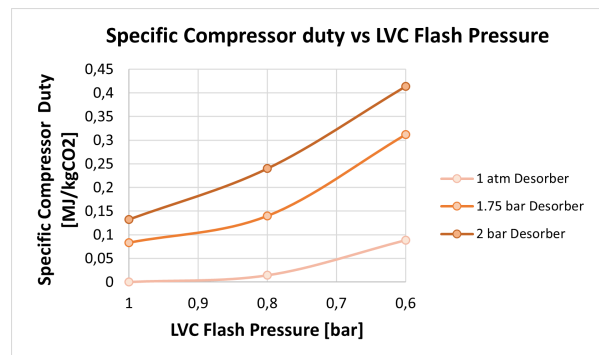


Figure 4.28: Specific compander duty as a function of LV-flash pressure.

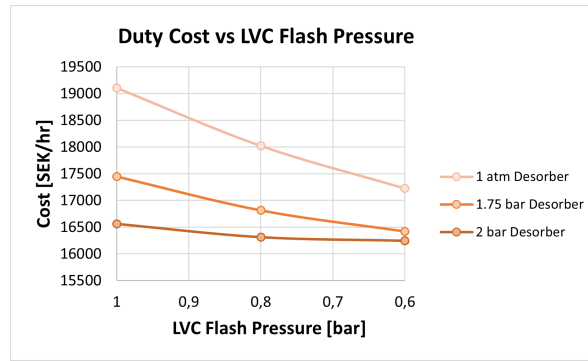


Figure 4.29: Total duty cost as a function of LV-flash pressure.

Figure 4.27 shows how the specific heat duty decreases with decreasing LV-flash pressure, reaching its lowest point for 0.6 bar LV-flash pressure for the highest desorber pressure, 2 bar. However, a lower LV-flash pressure results in a higher electricity duty due to the larger pressure difference in the compressor. The increasing compressor duty with decreasing LV-flash pressure and increasing desorber pressure can be seen in Figure 4.28. The third plot, Figure 4.29, shows that the lowest cost is associated to the 0.6 bar LVC with 2 bar pressured desorber. Hence, the decreased reboiler duty for 0.6 bar LVC compensates for the increased compressor duty resulting in the lowest cost. Since desorber pressures above 2 bar were ignored due to convergence issues, no cost-optimum is found as for HPC in Section 4.1.8. Thus, one would expect that the cost starts to increase somewhere above 2 bar with the current duty price assumptions provided by VEAB. A higher electricity price would lead to a lower optimal desorber pressure and higher a LV-flash pressure.

4.2.7 Intercooling

Intercooling was implemented to investigate if the specific heat duty could be decreased. The results presented in Figures 4.30 and 4.31 were obtained using an intercooler which cooled the flow to 50 °C at absorber stage number 8. Figures 4.30 and 4.31 illustrate how the specific heat duty and rich loading varies with intercooling to liquid ratio (IC/L). IC/L is thus a percentage of how much of the liquid stream that is intercooled in the absorber.

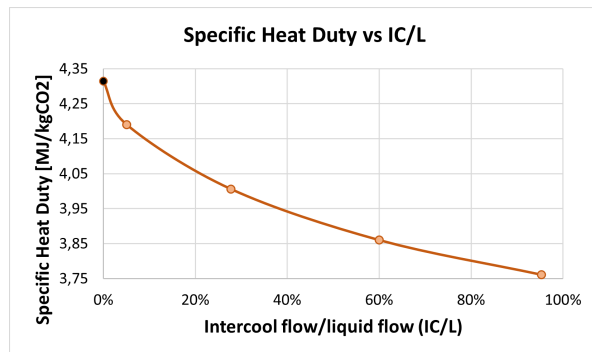


Figure 4.30: Specific heat duty as a function of intercooling ratio (IC/L).

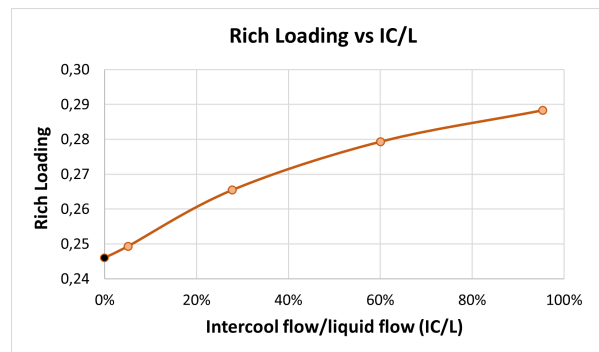


Figure 4.31: Rich Loading as a function of intercooling ratio (IC/L).

Figure 4.30 shows how the specific heat duty decreases with increased intercooled flow (IC/L), reaching a minimum approaching 100% IC/L. This tendency originates from the increased rich loading that ICA gives rise to, which can be seen in Figure 4.31. By cooling the hot solvent in the absorber and re-circulating it on the same stage, the CO₂ absorption is increased and a higher rich loading is reached. This higher rich loading enables a lower L/G ratio and they together result in a decreased reboiler duty. Hence, a high IC/L ratio is favoured.

There is another parameter which affects the result of intercooling, and that is the stage number for intercooling. Figure 4.32 illustrates how the specific heat duty changes with stage number. Note that stage number 1 is the top and stage number 20 is the bottom of the absorber. Stages above 16 were not evaluated due to convergence issues and time limitations.

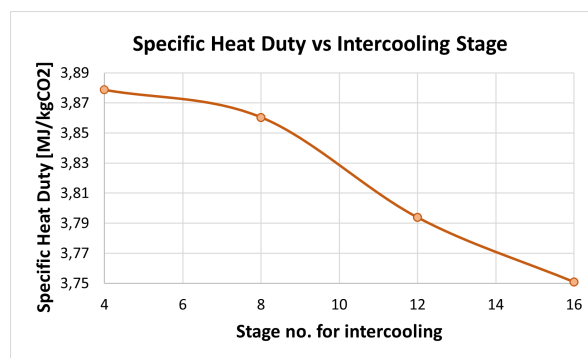


Figure 4.32: Specific heat duty for different intercooling stages using 60% IC/L

The conclusion that can be drawn from Figure 4.32 is that the specific heat duty decreases with increased stage number. Thus, the most optimal intercooling case is 100% IC/L at stage 16.

4.2.8 Optimized MDEA/DEA Model

The optimized HPC model was downsized in order to match the 80 % flooding approach. Thus, the absorber and desorber for the optimized MDEA/DEA was downsized accordingly. The final settings of the optimized downsized model are presented in Table 4.33 and Figure 4.2.8 illustrates the Aspen Plus model. The resulting duties and duty cost for the optimized model are presented in Table 4.4.

Table 4.3: MDEA/DEA optimized downsized model settings.

Optimized Downsized Model Settings	
Absorber Diameter	6.02 meters
Desorber Diameter	4.12 meters
Column Heights	20 meters
Number of Stages in Columns	20
Lean Solvent Inlet Temperature	45 °C
Lean Solvent Loading	0.02
MDEA Concentration	15 wt%
DEA Concentration	25 wt%
Desorber Pressure	2 Bar
LV-Flash Pressure	0.6 Bar
Intercooling Temperature	50 °C
Intercooling Stage no.	16
Intercooled/liquid flow ratio (IC/L)	99 %

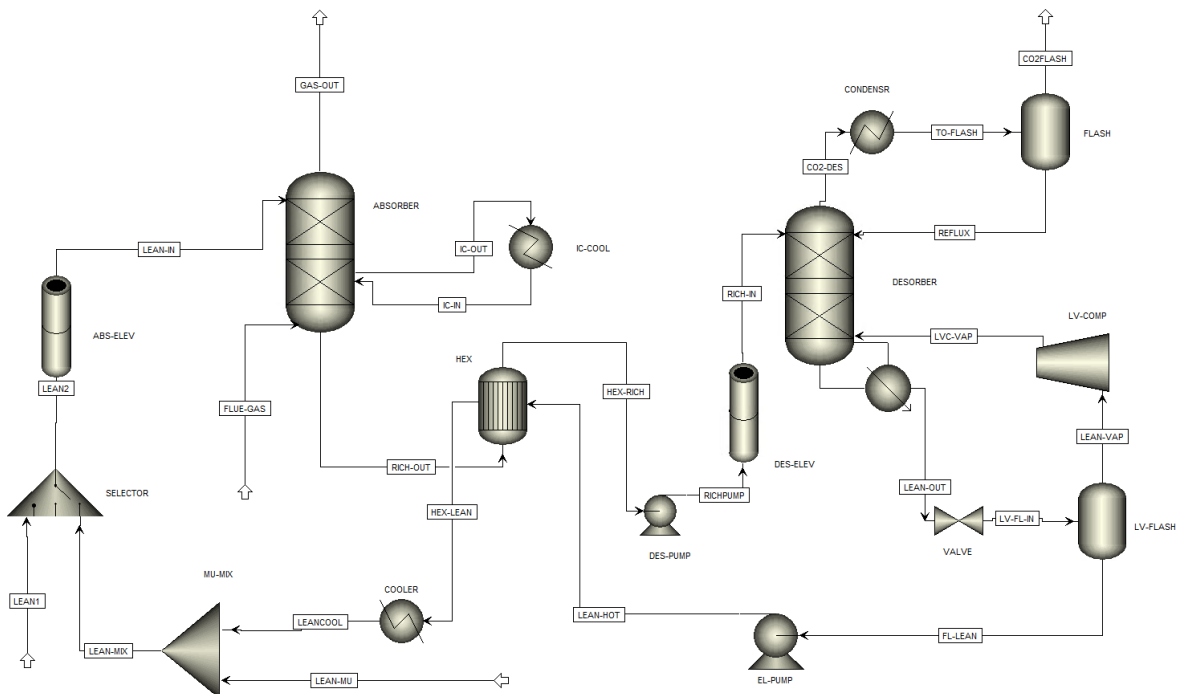


Figure 4.33: Aspen Plus MDEA/DEA optimized model.

Table 4.4: MDEA/DEA optimized downsized model results.

Optimized Downsized Model Results	Full Load	Half Load
L/G Ratio	4.07	3.40
Lean Solvent Make-up	1.55 %	2.29 %
Reboiler Duty	28.01 MW	14.28 MW
Specific Heat Duty	2.49 MJ/kgCO ₂	2.48 MJ/kgCO ₂
LVC Duty	3.52 MW	1.69 MW
Specific LVC Duty	0.31 MJ/kgCO ₂	0.29 MJ/kgCO ₂
HEX Duty	23.4 MW	11.3 MW
Condenser Duty	3.83 MW	1.92 MW
Cooler Duty	12.15	5.71
Intercooler Duty	5.42 MW	2.53 MW
Total Pump Duty	0.21 MW	0.10 MW
Carbon Capture Duty Cost	13 445 SEK/hr	6 643 SEK/hr
Liquefaction Compression Duty	4.94 MW	2.65 MW
Liquefaction DH Recovery	4.71 MW	2.53 MW
Total Duty Cost	16 407 SEK/hr	8 202 SEK/hr

Comparing with the base case, the optimized model had a significantly lower specific heat duty. The base case had a specific heat duty of 4.87 MJ/kgCO₂ while the optimized model had a specific heat duty of 2.49 MJ/kgCO₂. This specific heat duty decrease is the result of changing parameters to optimal ones while implementing LVC and intercooling (ICA). However, the obtained specific heat duties deviate from literature. Appendix D lists other literatures' estimated specific heat duties for MDEA and DEA alone, since no representative literature using a MDEA/DEA mix was found. Those literature values lay around 3 MJ/kgCO₂ for both amines and are obtained from a general technology setup, i.e. a setup like the base case model. The base case model's specific heat duty lies significantly above 3 MJ/kgCO₂, indicating that the Aspen Plus model is deviating from other's work and perhaps reality. The optimized model result lays closer to the literature values but since it has LVC and ICA implemented, the values cannot be compared. Hence, both of the Aspen Plus models overestimate the reboiler duty giving rise to higher specific heat duties than expected.

Nevertheless, when comparing the MDEA/DEA model's result to the HPC model's result it is noticeable that HPC might be the favourable choice. Despite HPC's higher electricity usage, 3765 SEK/hr of the total duty cost is saved when using the HPC solvent due to its significant lower reboiler duty. The next section will investigate the heat integration possibilities for the HPC and MDEA/DEA optimized models to evaluate their integration potential to VEAB's CHP plant.

5

Heat Integration

The heat integration begins with Section 5.1 which gives an estimation of how much of the excess heat within the CCS processes that can be recovered to the CHP plant's DH network. The following section, Section 5.2 investigates how a potential integration of CCS would affect the CHP plant performance and which type of CCS process that would be more favourable in that regard.

5.1 Heat Integration within CCS

In order to investigate how the implementation of CCS affects the CHP performance, an overall heat integration was performed. First, an estimation of the amount of available heat from the capture processes was made using the methodology described in Section 3.3. From this, the possible heat recovered from the capture and liquefaction processes to the DH network could be obtained. The recovered heat and the power need for the MDEA/DEA and HPC models can be seen in Table 5.1 and Table 5.2 respectively.

Table 5.1: Heat integration for MDEA/DEA capture process.

	Full Load		Half Load	
	CC Recovered Heat [MW]	Power need [MW]	CC Recovered Heat [MW]	Power need [MW]
Direct from CC	3.8	3.7	1.9	1.7
Heat Pump 1	17.0	4.9	6.8	2.0
Heat Pump 2	7.4	2.0	2.7	0.7
Liquefaction	4.7	4.9	2.5	2.6
Total	32.9	15.5	13.9	7.0

Table 5.2: Heat integration for HPC capture process.

	Full Load		Half Load	
	CC Recovered Heat [MW]	Power need [MW]	CC Recovered Heat [MW]	Power need [MW]
Direct from CC	16.3	11.8	7.1	6.2
Liquefaction	4.6	4.0	2.4	2.4
Total	20.9	15.8	9.5	8.6

Comparing Table 5.2 and Table 5.1 it is evident that MDEA/DEA has higher heat recovery possibilities whileas the power consumption is close to the same for both processes. This tendency can be seen for both full load and half load. The following section will investigate the heat integration to the CHP plant and evaluate how it affects its performance.

5.2 Integration of CCS to the CHP Plant

As been previously stated in Section 1.1, VEAB uses two different blocks to meet the DH demand, one is Sandvik 3 (SV3) and the other is Sandvik 2 (SV2). The idea is that the capture process will be connected to SV3 whereas SV2 will be used to cover the DH demand that is left. By using CHP data from VEAB, the fuel input, DH output and power output for each block could be calculated. The data corresponding to SV3 and SV2 can be found in Appendix C. To get an idea of how the CCS performance and heat integration are affected by seasons, two cases were investigated. One case for winter season, corresponding to full load, and one for summer season which corresponds to half load. Section 5.2.1 investigates the full load case while Section 5.2.2 investigates the half load case.

5.2.1 Full Load

In the winter, when SV3 runs at full load, the DH demand is assumed to be 119.7 MW based on data from VEAB. Since extraction of steam to the reboiler leads to a decrease in the power and DH output, this loss must be accounted for in the heat integration. The power loss was calculated by multiplying the extracted steam flow with the the enthalpy loss, i.e. the enthalpy difference between the extracted steam and LP steam. Due to the fact that LP steam is the last extraction point in the steam turbine, it means that DH production is also affected. By assuming that the extracted steam corresponds to the same loss of steam flow exiting the turbine, the loss in DH effect could also be calculated. The obtained result for full load can be seen in Table 5.3.

Table 5.3, includes three columns. The first column corresponds to the CHP baseline without CCS, the second corresponds to the CHP with HPC implemented on SV3 and the third column corresponds to the CHP with MDEA/DEA implemented on SV3. To compare the capture technologies' performances, sales has been calculated for each case and column. The sales only include the expected income from selling the power output for 600 SEK/MWhr and DH output for 250 SEK/MWhr (specified values from VEAB). To get a more representative value, the power and DH sales per fuel input ($\text{SEK}/\text{MW}_{fuel} \cdot \text{hr}$) were calculated. Note that the sales values are only measures for comparing the technologies and not actual representative sales income for VEAB's SV2 and SV3. Also, CHP efficiencies were calculated according to the equations in Section 2.1.1.

Table 5.3: Result from heat integration for full load (winter case), assuming DH demand of 119.7 MW.

	CHP Baseline Full Load	CHP with HPC Full Load	CHP with MDEA/DEA Full Load
Heat Recovery From CC [MW]	-	20.9	32.9
CC Power Consumption [MW]	-	15.8	15.5
Power Loss Due To Steam Extraction [MW]	-	1.1	3.8
Direct DH Loss Due To Steam Extraction [MW]	-	6.0	21.0
<hr/>			
SV3 Fuel Input [MW]	116.7	116.7	116.7
SV3 DH Output [MW]	89.0	83.0	68.0
SV3 Power Output [MW]	36.6	19.6	17.3
<hr/>			
SV2 Fuel Input [MW]	51.4	23.7	29.2
SV2 DH Output [MW]	30.7	15.7	18.7
SV2 Power Output [MW]	13.5	3.7	5.6
SV2 Load [%]	50.0	22.9	28.3
<hr/>			
Total Fuel Input [MW]	168.1	140.4	145.9
Total DH Output [MW]	119.7	119.7	119.7
Total Power Output [MW]	50.1	23.3	22.9
<hr/>			
Power-to-Heat Ratio (α)	0.42	0.19	0.19
η_{el} [%]	30.0	16.6	15.7
η_{tot} [%]	101.0	101.9	97.8
<hr/>			
Power + DH Sales [SEK/hr]	59 937	43 911	43 665
Power + DH Sales per Fuel Input [SEK/MW_{fuel} ·hr]	357	313	299

It can be noted from Table 5.3 that HPC and MDEA/DEA have about the same power consumption, whereas MDEA/DEA has a higher power loss and DH loss as a result of a larger steam extraction to the reboiler. This is the effect of MDEA/DEA's higher reboiler duty and thus higher steam consumption, which results in SV3 having a lower DH and power output for MDEA/DEA compared to HPC. However, by changing the focus to SV2 DH output, it can be seen that the difference between HPC and MDEA/DEA is only 3 MW. These 3 MW is the result of MDEA/DEA's larger heat recovery possibilities compared to HPC. Meaning that the recovered heat from MDEA/DEA covers up enough of the DH loss to catch up with HPC's performance.

Since SV2 is adjusted to only meet the DH demand, the total power output is not accounted for. According to Table 5.3, the total power output for VEAB would decrease to below half of its original value if CCS would be implemented with this integration at full load. This effect is also noticeable for the half load case in Table 5.4, where the power output goes from 15 MW to 6 MW when implementing CCS. It is also important to note that the minimum load of SV2 is 35%, so in the cases where CCS is implemented the SV2 load subceeds the minimum. This problem could be solved by using VEAB's DH accumulation tank.

Focusing the attention to the power-to-heat ratio (α), it can be seen that this parameter is almost the same for HPC and MDEA/DEA. α being close to the same for both technologies is expected since the total DH output is the same for both technologies whereas the total power output differs slightly, but not enough to be seen with two decimals. The same tendency can be recognized for the electrical efficiency (η_{el}) since the fuel input is kept constant throughout the calculations. The total efficiency (η_{tot}) however differs more. MDEA/DEA has an η_{tot} of 97.8% meanwhile HPC has a value of 101.9% and is thus closer, even above, the η_{tot} for the CHP baseline. Note that the total efficiency can overcome 100% due to the flue gas condensation, which is accounted for in all the calculations.

It can be seen in Table 5.3 that around 50 SEK/MW_{fuel} · hr would be lost when implementing CCS at full load. This is the result of a decreased electrical output when implementing CCS. The difference in sales between HPC and MDEA/DEA is however smaller. Around 14 SEK/MW_{fuel} · hr would be saved if HPC would to be implemented instead of MDEA/DEA at full load.

5.2.2 Half Load

In the summer, SV3 is assumed to be running at half load while the DH demand is 17.5 MW. Due to the low DH demand during summer, SV3 is sufficient to cover the demand. Hence, SV2 is not needed and therefore not included in the integration for half load. Also, as a result of the low DH demand, cooling will be needed to separate the excess heat from SV3. Except from these notes, the integration was made using the same approach as described in Section 5.2.1. The obtained result can be seen in Table 5.4 on the following page.

Table 5.4: Result from heat integration for half load (summer case), assuming DH demand of 17.5 MW.

	CHP Baseline Half Load	CHP with HPC Half Load	CHP with MDEA/DEA Half Load
Heat Recovery From CC [MW]	-	9.5	13.9
CC Power Consumption [MW]	-	8.6	7.0
Power Loss Due To Steam Extraction [MW]	-	0.5	1.9
Direct DH Loss Due To Steam Extraction [MW]	-	2.9	11.1
<hr/>			
SV3 Fuel Input [MW]	58.3	58.3	58.3
SV3 DH Output [MW]	46.4	43.5	35.3
SV3 Power Output [MW]	14.9	5.9	6.0
<hr/>			
Total Fuel Input [MW]	58.3	58.3	58.3
Total DH Output [MW]	46.4	53.0	49.3
Total Power Output [MW]	14.9	5.9	6.0
Cooling of Excess DH Heat [MW]	28.9	35.5	31.8
<hr/>			
Power-to-Heat Ratio (α)	0.32	0.11	0.12
η_{el} [%]	25.6	10.1	10.2
η_{tot} [%]	105.1	101.0	94.7
<hr/>			
Power + DH Sales [SEK/hr]	13 324	7 894	7 960
Power + DH Sales per Fuel Input [SEK/MW_{fuel} ·hr]	228	135	136

Similar tendencies as for full load can be seen in the half load results presented in Table 5.4. The power and DH loss due to steam extraction are higher for MDEA/DEA than for HPC, hence the DH output for SV3 is also lower. However, the DH demand is only 17.5 MW during summer, hence there is no need for operating SV2. Instead, cooling of the excess heat is needed to meet the DH demand.

The total power output from MDEA/DEA is slightly higher than for HPC, which results in MDEA/DEA having higher α and higher η_{el} . In addition, it is assumed that the DH demand of 17.5 MW is the only amount of DH that can be sold. Hence, MDEA/DEA will have slightly higher sales due to its higher power output. The difference in sales between MDEA/DEA and HPC is however only 1 SEK/MW_{fuel} · hr. Note that the cooling cost has not been included in the sales calculations.

5.3 Heat Integration Summary

Comparing all the results from the heat integration, it is evident that implementing CCS would give rise to sales losses due to a decrease in power output, which is expected. Thus, it is more important to evaluate which of the technologies that would be more suitable to implement. HPC is the more favourable technology for full load due to its lower reboiler duty and the resulted higher power output. Whereas MDEA/DEA is the more favourable choice for half load due to its slightly higher power output and lower cooling demand. Overall, HPC seems to be the more promising technology given the assumptions used in this thesis. HPC has not only a higher overall sales income but also a significantly lower reboiler duty and a higher total efficiency compared to MDEA/DEA. Note once again that the sales calculations are very simplified and only account for the power and DH sales without including anything else. A more detailed cost estimation would provide a more thorough comparison and more representative results.

6

Conclusions

In this thesis the implementation of two different post-combustion carbon capture technologies at VEAB's CHP plant has been investigated and compared. By conducting simulations in Aspen Plus a heat integration could be performed to evaluate the effect of the carbon capture technologies on the CHP plant performance.

The parameter studies laid ground for the optimization of the models in order to minimize the energy demand as well as favouring the heat integration to the DH network. From the parameter studies it could be observed that certain process conditions favoured the minimization of the energy demand for the different technologies. It could also be concluded that process modifications such as lean vapour compression and intercooled absorption gave rise to a lower energy demand.

The results from the optimized Aspen Plus models of the technologies were then used to perform the heat integration to VEAB's DH network. The results from the heat integration facilitated the comparison between the different technologies and their effect on the CHP plant performance. It could be concluded that at a half load scenario the technologies performed similarly. However, at a full load scenario the HPC technology seemed to be the more favourable option. Since the CHP plant operates at a high load over the major part of the year, the HPC technology is the preferred option based on the results in this thesis.

6.1 Future Work

It is important to note that the results in this thesis are based on software simulations, which can only represent reality to a certain extent. To get a more accurate understanding of how the carbon capture models perform in reality it would be recommended to carry out real experiments, such as implementing a pilot plant. Another possible improvement of the results could be to perform extensive techno-economic analyses, rather than coarse sales calculations. A sensitivity analysis would also provide valuable information regarding the robustness of the two carbon capture technologies.

Bibliography

- [1] NOAA Climate.gov, *Climate change: Atmospheric carbon dioxide*. [Online]. Available: <https://www.climate.gov/news-features/understanding-climate/climate-change-atmospheric-carbon-dioxide> (visited on 01/24/2023).
- [2] Fosbøl P., von Solms N., Gladis A., Thomsen K. and Kontogeorgis G. M., *Process Systems and Materials for CO₂ Capture: Modelling, Design, Control and Integration*. John Wiley & Sons Ltd., 2017, ISBN: 978-1-4612-2272-9. [Online]. Available: <https://onlinelibrary.wiley.com/doi/abs/10.1002/9781119106418.ch2>.
- [3] United States Environmental Protection Agency, *What is CHP?* [Online]. Available: <https://www.epa.gov/chp/what-chp> (visited on 01/25/2023).
- [4] United States Environmental Protection Agency, *CHP benefits*. [Online]. Available: <https://www.epa.gov/chp/chp-benefits> (visited on 01/31/2023).
- [5] Thorin E., Sandberg J. and Yan J., “Combined heat and power,” *Handbook of Clean Energy Systems*, 2015. DOI: 10.1002/9781118991978.hces021.
- [6] Sipilä K., Pursiheimo E., Savola T., Fogelholm C. J., Keppo I. and Ahtila P., “Small-scale biomass CHP plant and district heating,” *VTT Tiedotteita - Valtion Teknillinen Tutkimuskeskus*, vol. 2301, pp. 3–129, 2005, ISSN: 1455-0865. DOI: https://www.researchgate.net/publication/289304700_Small-scale_biomass_CHP_plant_and_district_heating.
- [7] U.S. Department of Energy, *Industrial heat pumps for steam and fuel savings*. [Online]. Available: <https://www.energy.gov/eere/amo/articles/industrial-heat-pumps-steam-and-fuel-savings> (visited on 04/06/2023).
- [8] National Energy Technology Laboratory, *9.1.1. Carbon dioxide capture approaches*. [Online]. Available: <https://netl.doe.gov/research/coal/energy-systems/gasification/gasifipedia/capture-approaches> (visited on 01/24/2023).
- [9] Liu H., Idem R. and Tontiwachwuthikul P., *Post-combustion CO₂ Capture Technology*. Springer Cham, 2019, ISBN: 978-3-030-00922-9. [Online]. Available: https://link-springer-com.proxy.lib.chalmers.se/chapter/10.1007/978-3-030-00922-9_1.
- [10] Aghel B., Janati S., Wongwises S. and Safdari Shadloo M., “Review on CO₂ capture by blended amine solutions,” *International Journal of Greenhouse Gas Control*, vol. 119, p. 103715, 2022. DOI: <https://doi.org/10.1016/j.ijggc.2022.103715>.
- [11] Finney K. N., Akram M., Diego E. M., Yang X. and Pourkashanian M., *Bioenergy with Carbon Capture and Storage - Using Natural Resources for Sustainable Development*. Academic Press, 2019, ISBN: 978-0-12-816229-3. [Online]. Avail-

- able: <https://www.sciencedirect.com/book/9780128162293/bioenergy-with-carbon-capture-and-storage>.
- [12] Dutcher B., Fan M. and Russell A. G., “Amine-based CO₂ capture technology development from the beginning of 2013—a review,” *ACS Applied Materials & Interfaces*, 2015. DOI: 10.1021/am507465f.
- [13] Voice A. K., Hill A., Fine N. A. and Rochelle G. T., “Nitrosamine formation and mitigation in blended amines for CO₂ capture,” *International Journal of Greenhouse Gas Control*, vol. 39, pp. 329–334, 2015. DOI: <https://www.sciencedirect.com/science/article/pii/S1750583615001930>.
- [14] European Medicines Agency, *Nitrosamine impurities*. [Online]. Available: <https://www.ema.europa.eu/en/human-regulatory/post-authorisation/referral-procedures/nitrosamine-impurities> (visited on 02/01/2023).
- [15] Puxty G., Maeder M. and Rochelle G. T., *Absorption-Based Post-Combustion Capture of Carbon Dioxide*. Woodhead Publishing, 2016, ISBN: 978-0-08-100514-9. [Online]. Available: <https://www.sciencedirect.com/book/9780081005149/absorption-based-post-combustion-capture-of-carbon-dioxide>.
- [16] Ware G. W. and et al, *Reviews of Environmental Contamination and Toxicology*. Springer-Verlag, 1997, ISBN: 9781119106418. [Online]. Available: <https://link.springer.com/content/pdf/10.1007/978-1-4612-2272-9.pdf?pdf=button>.
- [17] Aghel B., Sahraie S., Heidaryan E. and Varmira K., “Experimental study of carbon dioxide absorption by mixed aqueous solutions of methyl diethanolamine (MDEA) and piperazine (PZ) in a microreactor,” *Process Safety and Environmental Protection*, vol. 131, pp. 152–159, 2019. DOI: <https://doi.org/10.1016/j.psep.2019.09.008>.
- [18] Borhani T. N., Babamohammadi S., Khallagi N. and Zhang Z., “Mixture of piperazine and potassium carbonate to absorb CO₂ in the packed column: Modelling study,” *Fuel*, vol. 308, p. 122 033, 2022. DOI: <https://doi.org/10.1016/j.fuel.2021.122033>.
- [19] European Chemicals Agency (ECHA), *Substance infocard - piperazine*. [Online]. Available: <https://echa.europa.eu/sv/substance-information/-/substanceinfo/100.003.463> (visited on 02/13/2023).
- [20] Xue B., Yu Y., Chen J., Luo X. and Wang M., “A comparative study of mea and dea for post-combustion CO₂ capture with different process configurations,” *International Journal of Coal Science Technology*, vol. 4, pp. 15–24, 2017. DOI: <https://doi.org/10.1007/s40789-016-0149-7>.
- [21] Zhao X., Smith K. H., Simioni M. A., Tao W., Kentish S. E., Fei W. and Stevens G. W., “Comparison of several packings for CO₂ chemical absorption in a packed column,” *International Journal of Greenhouse Gas Control*, vol. 5, pp. 1163–1169, 2011, ISSN: 1750-5836. DOI: 10.1016/j.ijggc.2011.07.006.
- [22] Bryngelsson M. and Westermark M., “CO₂ capture pilot test at a pressurized coal fired chp plant,” *Energy Procedia*, vol. 1, pp. 1403–1410, 2009. DOI: <http://dx.doi.org/10.1016/j.egypro.2009.01.184>.
- [23] Hu G., Nicholas N. J., Smith K. H., Mumford K. A., Kentish S. E. and Stevens G. W., “Carbon dioxide absorption into promoted potassium carbonate solutions: A review,” *International Journal of Greenhouse Gas Control*, vol. 53, pp. 28–40,

- 2016, ISSN: 1750-5836. DOI: <http://dx.doi.org/10.1016/j.ijggc.2016.07.020>.
- [24] Smith K. H., Anderson C. J., Tao W., Endo K., Mumford K. A., Kentish S. E., Qader A., Hooper B. and Stevens G. W., “Pre-combustion capture of CO₂—results from solvent absorption pilot plant trials using 30 wt% potassium carbonate and boric acid promoted potassium carbonate solvent solutions: A review,” *International Journal of Greenhouse Gas Control*, vol. 10, pp. 64–73, 2012, ISSN: 1750-5836. DOI: <http://dx.doi.org/10.1016/j.ijggc.2012.05.018>.
- [25] Léonard G. and Heyen G., “Modeling post-combustion CO₂ capture with amine solvents,” *Computer Aided Chemical Engineering*, vol. 29, pp. 1768–1772, 2011. DOI: <https://doi.org/10.1016/B978-0-444-54298-4.50132-X>.
- [26] Lee U., Yang S., Su Jeong Y., Lim Y., Seob Lee C. and Han C., “Carbon dioxide liquefaction process for ship transportation,” *Industrial & Engineering Chemistry Research*, vol. 51, pp. 15 122–15 131, 2012. DOI: dx.doi.org/10.1021/ie300431z.
- [27] Deng H., Roussanaly S. and Skaugen G., “Techno-economic analyses of CO₂ liquefaction: Impact of product pressure and impurities,” *International Journal of Refrigeration*, vol. 103, pp. 301–315, 2019. DOI: <https://doi.org/10.1016/j.ijrefrig.2019.04.011>.
- [28] Ali M., Kumar Jha N., Pal N., Keshavarz A., Hoteit H. and Sarmadivaleh M., “Recent advances in carbon dioxide geological storage, experimental procedures, influencing parameters, and future outlook,” *Earth-Science Reviews*, vol. 225, p. 103 895, 2022. DOI: <https://doi.org/10.1016/j.earscirev.2021.103895>.
- [29] Northern Lights JV DA, *What we do*. [Online]. Available: <https://norlights.com/what-we-do/> (visited on 02/06/2023).
- [30] Al-Matar A., “Selecting fluid packages (thermodynamic model) for HYSYS/ Aspen Plus/ ChemCAD process simulators,” 2015. DOI: <http://dx.doi.org/10.13140/RG.2.1.3461.4487>.
- [31] Kim K. I., Ri J. H., Kim S. E. and Kim I. H., “Estimation of interaction parameters of electrolyte NRTL model based on NaCN and Na₂CO₃ solubility in water–ethanol mixed solvent and process simulation for separation of NaCN/Na₂CO₃,” *SN Applied Sciences*, vol. 2, p. 2112, 2020. DOI: <https://doi.org/10.1007/s42452-020-03914-5>.
- [32] Aspen Tech, *Thermodynamics university modules*. [Online]. Available: https://esupport.aspentech.com/S%5C_Article?id=141651 (visited on 04/25/2023).
- [33] Zevenhoven R. and Kilpinen P., *Control of pollutants in flue gases and fuel gases*. Helsinki University of Technology, 2005, ISBN: 951-22-5527-8. [Online]. Available: <http://users.abo.fi/rzevenho/gasbook.html>.
- [34] Aspen Tech Example, *ELECNRTL rate based K2CO3 model*.
- [35] Aspen Tech Example, *ELECNRTL rate based DEA+MDEA model*.
- [36] Aspen Tech, *Aspen rate-based simulation*. [Online]. Available: <https://knowledgecenter.aspentech.com/help/Aspen%5C%20Plus/12/apwn.htm#../Subsystems/userguide2/Content/html/ratesep.htm> (visited on 04/25/2023).

-
- [37] Kohl A. L. and Nielsen R. B., *Gas Purification*. Gulf Professional Publishing, 1997, ISBN: 978-0-88415-220-0. [Online]. Available: <https://www.sciencedirect.com/science/article/pii/B9780884152200500057>.
- [38] Biermann M., Normann F., Johnsson F., Hoballah R. and Onarheim K., “Capture of CO₂ from steam reformer flue gases using monoethanolamine: Pilot plant validation and process design for partial capture,” *Industrial Engineering Chemistry Research*, vol. 61, pp. 14305–14323, 2022. DOI: <https://doi.org/10.1021/acs.iecr.2c02205>.
- [39] Adu E., Zhang Y.D., Liu D. and Tontiwachwuthikul P., “Parametric process design and economic analysis of post-combustion CO₂ capture and compression for coal- and natural gas-fired power plants,” *Energies*, vol. 13, 2020. DOI: 10.3390/en13102519.
- [40] Gaertner S., Marx-Schubach T., Garderer M., Schmitz G. and Sterner M., “Techno-economic analysis of carbon dioxide separation for an innovative energy concept towards low-emission glass melting,” *Energies*, vol. 16, 2023. DOI: 10.3390/en16052140.
- [41] Moioli S., Pellegrini L. A., Romano M. C. and Giuffrida A., “Pre-combustion CO₂ removal in IGCC plant by MDEA scrubbing: Modifications to the process flow-sheet for energy saving,” *Energy Procedia*, vol. 114, 2017. DOI: <https://doi.org/10.1016/j.egypro.2017.03.1349>.
- [42] Moioli S., Giuffrida A., Gamba S., Romano M. C., Pellegrini L. and Lozza G., “Pre-combustion CO₂ capture by MDEA process in IGCC based on air-blown gasification,” *Energy Procedia*, vol. 63, 2014. DOI: <https://doi.org/10.1016/j.egypro.2014.11.220>.
- [43] Cui Q., Tu T., Ji L. and Yan S., “CO₂ capture cost saving through waste heat recovery using transport membrane condenser in different solvent-based carbon capture processes,” *Energy*, vol. 216, 2021. DOI: <https://doi.org/10.1016/j.energy.2020.119225>.
- [44] Ayithey F. K. et al, “Rate-based simulation study of boric acid promoted potassium carbonate capture system,” *IOP Conference Series: Materials Science and Engineering*, vol. 778, p. 012082, 2020. DOI: 10.1088/1757-899X/778/1/012082.
- [45] Roshan Kumar T., Beiron J., Biermann M., Harvey S. and Thunman H., “Plant and system-level performance of combined heat and power plants equipped with different carbon capture technologies,” *Applied Energy*, vol. 338, p. 120927, 2023. DOI: <https://doi.org/10.1016/j.apenergy.2023.120927>.

A

Liquefaction Model in Aspen Plus

The figure on the next page illustrates the liquefaction model that was simulated in Aspen Plus.

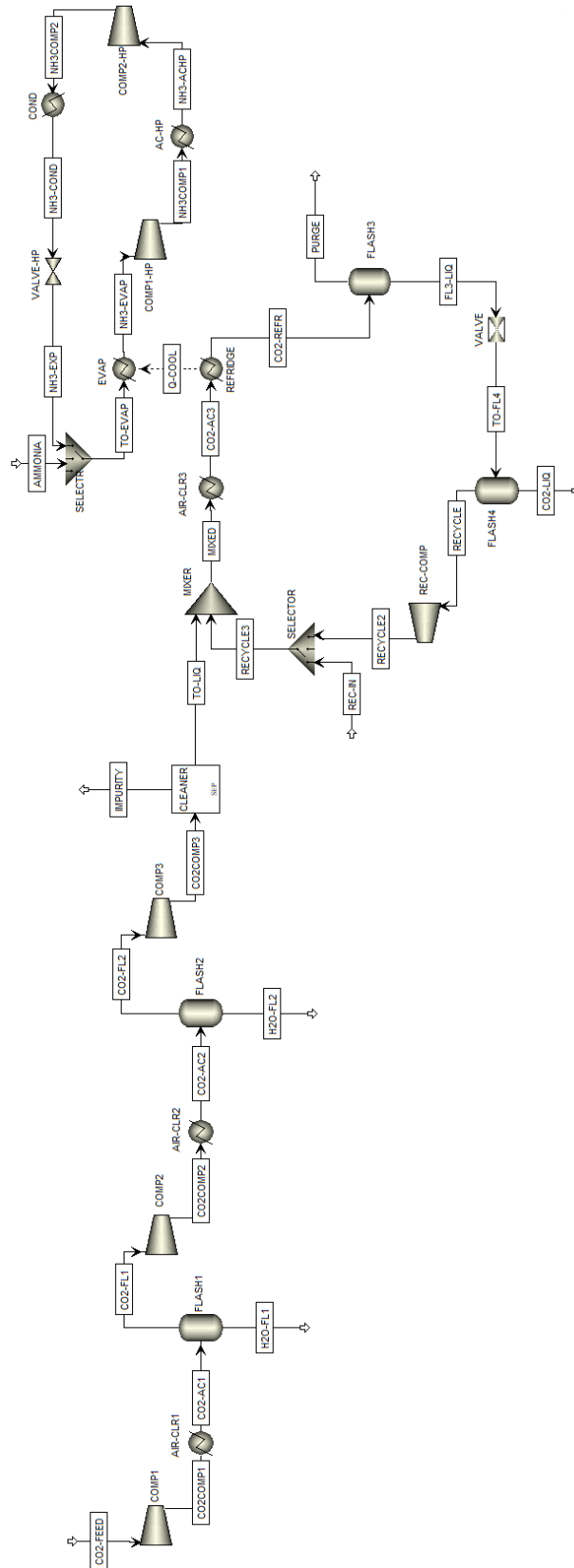


Figure A.1: Liquefaction model used for the HPC and MDEA/DEA models to obtain power and cooling need.

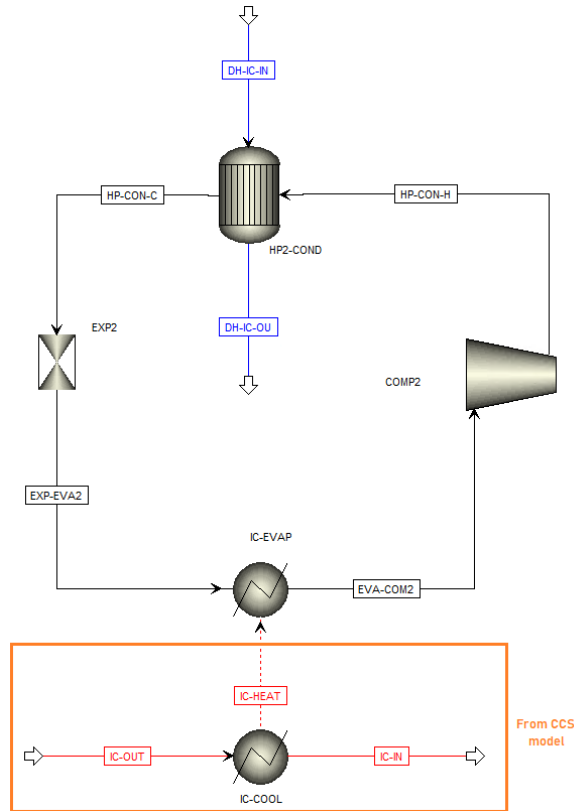


Figure B.2: Aspen Plus Heat Pump 2 model.

Table B.1: Result from MDEA/DEA heat integration of Heat Pumps.

	Unit name	Duties Full Load [MW]	Duties Half Load [MW]
From CCS-model	CONDENSR	3.83	1.89
	COOLER	12.15	4.87
	IC-COOL	5.42	1.99
Heat Pump 1	HP-COND-1	1.39	0.71
	HP-CON-2	15.63	6.14
	HP-EVAP	12.15	4.87
	COMP	4.88	1.98
Heat Pump 2	HP2-COND	7.38	2.72
	IC-EVAP	5.42	1.99
	COMP2	1.96	0.73
	Total heat recovered	24.40	9.57
	Total power need	6.84	2.71

C

CHP data for SV2 and SV3

The linear correlations in the following figures were used to calculate the heat and power output for SV3 and SV2. According to VEAB, the fuel efficiency in the boiler is 90%, hence the total fuel input was calculated by dividing "ågeffekt" with 0.9.

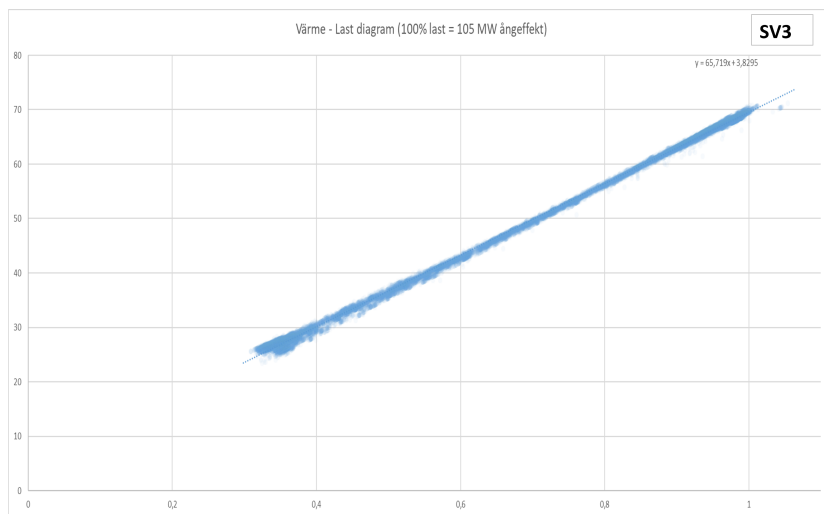


Figure C.1: Data for SV3 - District heating output (MW) vs load

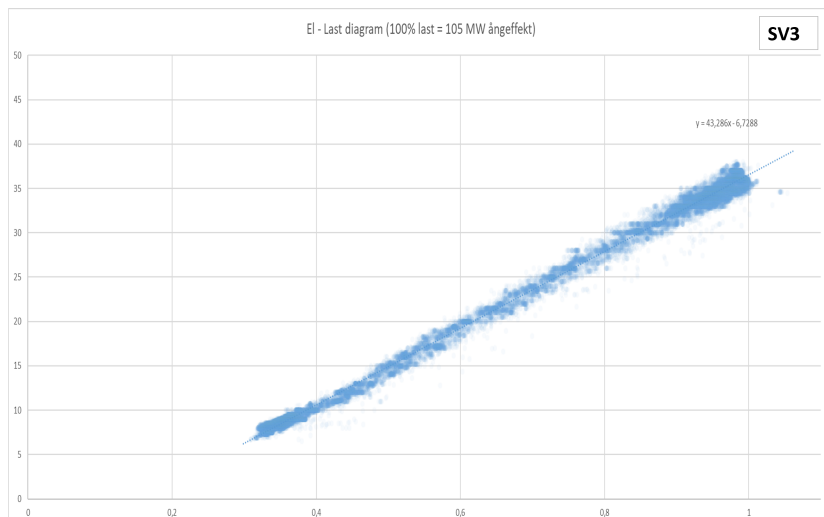


Figure C.2: Data for SV3 - Power output (MW) vs load

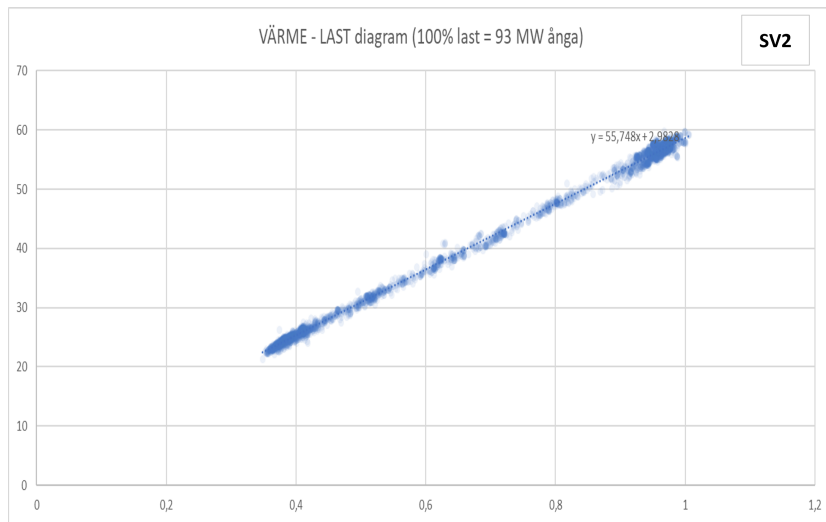


Figure C.3: Data for SV2 - District heating output (MW) vs load

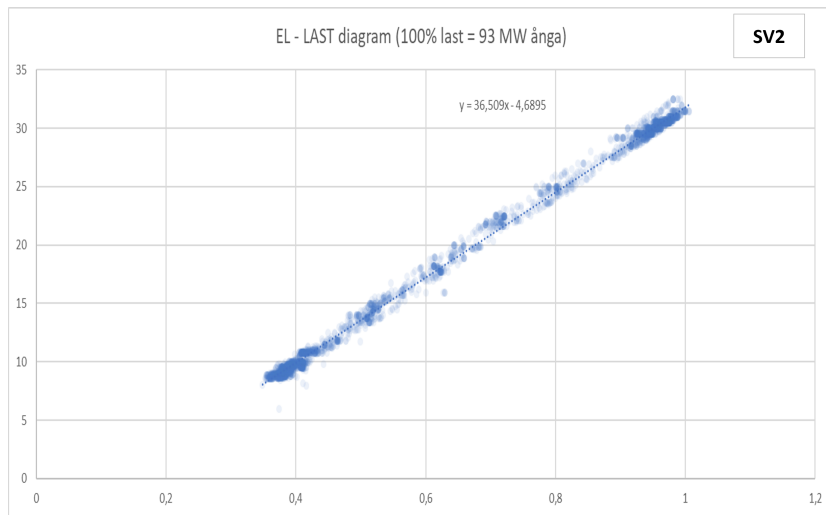


Figure C.4: Data for SV2 - Power output (MW) vs load

D

Specific Heat Duties from Literature

In Table D.1 different values for specific heat duties for different CCS technologies are presented.

Table D.1: Specific heat duty for solvent regeneration for MEA, MDEA, DEA and HPC capture technologies based on literature.*Uses pressurized absorption

Solvent	Specific heat duty (MJ/kg CO₂)	Capture rate (%)	Reference
30 wt% MEA	3.9	90	[39]
30 wt% MEA	3.4	90	[40]
50 wt% MDEA*	3.2	95	[41]
50 wt% MDEA*	3.0	87	[42]
DEA	ca 3	-	[43]
40 wt% HPC*	2.8	78	[44]
40 wt% HPC*	3.2	85	[44]
40 wt% HPC*	3.4	90	[45]

DEPARTMENT OF CHEMISTRY AND CHEMICAL ENGINEERING
CHALMERS UNIVERSITY OF TECHNOLOGY

Gothenburg, Sweden

www.chalmers.se



CHALMERS
UNIVERSITY OF TECHNOLOGY